

國立臺灣大學理學院物理學研究所

碩士論文

Department of Physics

College of Science

National Taiwan University

Master Thesis

一維奈米結構之二氧化錫的光導特性

Photocurrent of One-Dimensional SnO<sub>2</sub> Nanowires

林振華

Cheng-Hua Lin

指導教授：陳永芳 教授

Advisor: Yang-Fang Chen, Ph.D.

中華民國 97 年 6 月

June, 2008

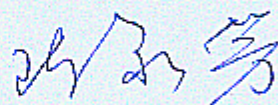
國立臺灣大學（碩）博士學位論文  
口試委員會審定書

一維奈米結構之二氧化錫的光導特性

Photocurrent of One-Dimensional Nanosized Structure of  
SnO<sub>2</sub>

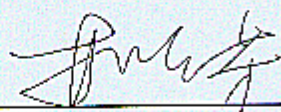
本論文係林振華君（R95222034）在國立臺灣大學物理學研究所  
完成之碩士學位論文，於民國 97 年 6 月 25 日承下列考試委員審查通  
過及口試及格，特此證明

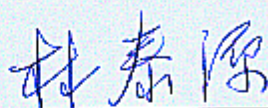
口試委員：



（簽名）

（指導教授）





# 致謝

能夠完成這篇論文，最要感謝的就是我的指導教授陳永芳老師。這兩年來因為您的指導以及鞭策下，我才能在半導體的實驗中獲得研究該有的態度及精神，更感激您給我實驗上充分的資源及支持，讓我能心無旁騖地專注在實驗上。

感謝張顏暉老師和梁啓德老師在 Group Meeting 時所給予許多寶貴的建議及指教；感激林麗瓊實驗室的博士後研究員陳瑞山學長在實驗上的所有諮詢以及協助，更要感謝學長宗德所給予的一切指導及幫助，也要感謝瀚葵不辭辛勞的帶我去電機系蒸鍍。此外，還要感謝半導體實驗室成員的眾位學長姊凱信、斯平、夏玉、仲良、志瑋、群雄、志銘、業岳、俊儀、奕任所提供的各種資訊及幫忙，並感謝同儕孟霖、中澤、彥嘉、威宏、函宇、宗玄、國裕、世豪、志彬、威仁和郁儒一起經歷的研究生生活。

最後感謝永遠陪在我身旁的家人，爸媽及兩位姊姊和小弟。雖然我們聚少離多，但感情仍然深厚。而你們永遠支持我，讓我能專心在課業上，振華所有的成就都是你們的功勞。

# Contents

摘要.....	III
Abstract.....	IV
List of figures.....	VI
<b>1. Introduction.....</b>	<b>1</b>
1-1 Introduction to Nanotechnology.....	1
1-2 Introduction to SnO <sub>2</sub> material.....	2
1-3 Photoconductivity.....	3
References.....	6
<b>2. Experimental instruments and details.....</b>	<b>8</b>
2-1 Scanning Electron Microscope.....	8
2-2 X-ray Diffraction.....	12
2-3 Raman Scattering.....	13
2-3-1 Stokes shift and Anti Stokes shift.....	14
2-3-2 Raman Scattering Apparatus.....	17
2-4 Experimental details and setups.....	20
2-4-1 Synthesization of SnO <sub>2</sub> nanowires .....	20
2-4-2 Fabrication of SnO <sub>2</sub> nanowires device.....	21
2-4-3 Two terminal I-V measurement.....	22
2-4-4 Photoconductivity measurement in air and in vacuum.....	22
2-5 Sputtering metallic nanoparticles.....	23
<b>3. High photocurrent gain in SnO<sub>2</sub> nanowires.....</b>	<b>31</b>
3-1 Introduction.....	31
3-2 Results and Discussion.....	32
3-3 Summary.....	43
References.....	44
<b>4. Photocurrent enhancement of SnO<sub>2</sub> nanowires through Au-nanoparticles decoration.....</b>	<b>46</b>
4-1 Introduction.....	46
4-2 Results and Discussion.....	47
4-3 Summary.....	57

References.....	58
<b>5. Conclusion.....</b>	<b>60</b>

## 摘 要

我們主要研究了二氧化錫一維奈米線 (nanowire) 的光導 (photocurrent) 特性。二氧化錫 ( $\text{SnO}_2$ ) 在奈米尺寸下擁有較高的表面積對體積比 (surface-to-volume ratio)，大幅增加了對光的靈敏度及吸收率。然而表面複雜的態卻會對光導造成巨大的影響。

我們將會報告由氣液固相製程所生成的  $\text{SnO}_2$  奈米線在紫外光波段擁有高效率的光轉電的能力。而以往所討論主宰  $\text{SnO}_2$  光導機制都只著重在表面氧分子吸附的電洞攫取，而忽略了因為能帶彎曲導致的電子電洞對分離所貢獻的光電流。而在真空時，由於氧分子吸附能力的降低，大大增長了電子電洞對存活的時間，進而大幅增加了光導率。

我們也參考了利用金屬粒子修飾增加  $\text{SnO}_2$  奈米線偵測活躍氣體靈敏度的模型來增加光導率。利用金屬粒子在  $\text{SnO}_2$  奈米線上形成蕭基屏障 (Schottky barrier) 增加能帶彎曲導致電子電洞對分離的效果更為顯著，有效增長電子電洞的生命期 (lifetime) 進而增加  $\text{SnO}_2$  奈米線的光導率。

# Abstract

In this thesis, the photocurrent of one-dimensional tin dioxide nanowires has been investigated. The mechanism responsible for photocurrent is explicated here and an alternative route to enhance photocurrent is provided. They are presented as follows.

## **I. High photocurrent gain in SnO<sub>2</sub> nanowires**

Unlike previous reports, the responsible mechanism of photocurrent in metal oxide nanostructures, always emphasize on the carrier trapping of charged oxygen molecules. Here we point out that space charges induced by surface defects does play a significant role, especially, for nanostructured materials with a large surface to volume ratio. The huge photoresponse gain with a value of about one hundred thousand detected in vacuum represents an outstanding example to illustrate out proposed mechanism. The study shown here provides a useful guideline to achieve photodetectors based on nanostructured materials with high sensitivity.

## **II. Photocurrent enhancement of SnO<sub>2</sub> nanowires through Au-nanoparticles decoration**

It is found the sensitivity of photoresponse of SnO<sub>2</sub> nanowires can be enhanced

by metallic decoration. The underlying mechanism is attributed to the formation of the Schottky junction on the nanowires surface in the vicinity of metallic nanoparticles. The increment in the barrier height and width of space charge region due to the existence of Schottky junctions increases the surface electric field and enhances the spatial separation effect, which then prolongs the lifetime of photoinduced electron and consequently increases the gain. The results shown here provide an alternative way for enhancing the photoresponse of semiconductor nanostructures, which should be useful for creating highly sensitive photodetectors.

Key words: Photocurrent, SnO<sub>2</sub>, nanowires, high gain, metal decoration.



## *List of Figures*

Fig. 2-1: Summary of the range of and spatial resolution of backscattered electrons, secondary electrons, X-ray, and Auger electrons for electrons incident on a solid, and etching the exposed portion of the materials. Electron trajectories, calculated with Monte Carlo techniques, also agree with these shapes.....	11
Fig. 2-2: The X-Ray Apparatus.....	13
Fig 2-3-1: Ideal model of Stokes and Anti-Stokes Raman scattering.....	15
Fig. 2-3-2: Jobin-Yvon T64000 Micro-Raman System.....	18
Fig. 2-3-3: Schematic of a Raman microscope. The microscope objective lens focuses the laser beam to a spot size of about $1 \mu\text{m}$ . Scattered light is transmitted through the beam splitter to the triple monochromator, giving the Raman spectrum of the selected region. Visible light from the illuminator is reflected from the sample to a video camera, giving a realtime image to the allow position of the probe beam. The sample can be moved on the x-y stage.....	19
Fig. 2-4: The setup of air and vacuum measurement system.....	23
Fig. 2-4-1: (a)(b) Scanning electron microscope image of $\text{SnO}_2$ NWs deposited on M-plane sapphire.....	25
Fig. 2-4-2: The corresponding (a) X-ray diffraction pattern and (b) Raman spectrum measured from the as-synthesized $\text{SnO}_2$ nanowires.....	26
Fig. 2-4-3: (a) Unit cell of the structure of $\text{SnO}_2$ . (b) Atomic displacement of atoms, viewed along the c axis, associated with Raman-active modes.....	27
Fig. 2-4-4: (a)(b) Various magnifying scanning electron microscope patterns of the morphologies of the fabricated $\text{SnO}_2$ nanobelts .....	28
Fig 2-4-5: Scanning electron microscope image of a single $\text{SnO}_2$ nanowire straddled with Ni/Au pad and the plug by the shadow mask method.....	29

Fig. 2-4-6: The SnO<sub>2</sub> Nanowire between two terminals exhibits perfect Ohmic characteristics.....30

Fig 2-5: Au-nanoparticles distribution on the Si substate.....30

Fig. 3-1: *I-V* characteristics of SnO<sub>2</sub> nanowire in ambient air.....38

Fig. 3-2: Photocurrent of SnO<sub>2</sub> nanowire with a bias 0.1V under different excitation intensity.....38

Fig. 3-3: (a) Photoconduction gain of SnO<sub>2</sub> nanowire as a function of illumination intensity. (b) Photocurrent of a SnO<sub>2</sub> nanowire as a function of excitation intensity...39

Fig. 3-4: Photoconduction gain of “short rise time” photocurrent versus different excitation intensity. ....40

Fig. 3-5: Photocurrent of a SnO<sub>2</sub> nanowire in air and in vacuum under the illumination of He-Cd laser with wavelength 325nm and excitation intensity of 100 W/m<sup>2</sup> in vacuum. ....40

Fig. 3-6: (a) Photocurrent of a SnO<sub>2</sub> nanowire under the illumination of He-Cd laser with wavelength 325nm in vacuum. (b) Photoconduction gain relative to excitation intensity in vacuum.....41

Fig 3-7: Photoresponse of the SnO<sub>2</sub> nanowire device under green laser illumination (532nm) with light intensity 40000 W/m<sup>2</sup>.....42

Fig. 4-1: *I-V* characteristics of SnO<sub>2</sub> nanowires with and without Au-nanoparticles in ambient air.....51

Fig. 4-2: (a) Scanning electron microscope (SEM) image of the Au-decorated SnO<sub>2</sub> nanowires.....51

Fig. 4-3: Photoresponse of SnO<sub>2</sub> nanowires by UV illumination under different

excitation intensity.....52

Fig. 4-4: Power dependence of pristine and Au-decorated SnO<sub>2</sub> nanowires.....53

Fig. 4-5: (a.) Accumulation of free electrons and upward band-bending on the surface. (b.) Au-nanoparticles result in a localized Schottky barrier in the vicinity of Au-nanoparticles, which will increase the height and the width of space charge region.....54

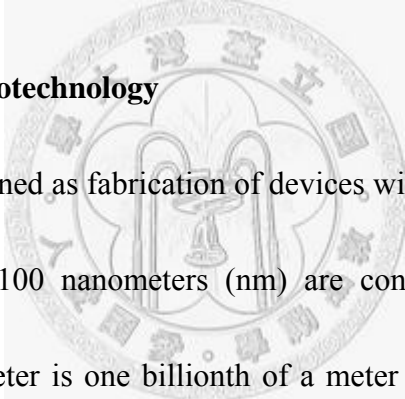
Fig. 4-6: Computer simulation of gain versus intensity and barrier height. An increase of the exponent  $\kappa$  and gain with increasing barrier height are obtained by this model.....55

Fig. 4-7: Photocurrent measurement in (a) pristine and (b) Au-decorated SnO<sub>2</sub> nanowires with an intensity of 53 W/m<sup>2</sup>.....56

# Chapter 1

## Introduction

### 1.1 Introduction to Nanotechnology



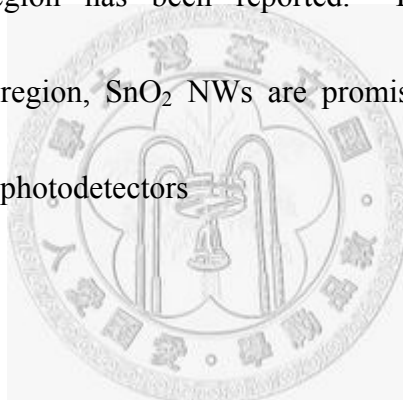
Nanotechnology is defined as fabrication of devices with molecular scale. Devices with feature sizes about 100 nanometers (nm) are considered to be products of nanotechnology. A nanometer is one billionth of a meter ( $10^{-9}$  m) and is the unit of length that is generally most appropriate for describing the size of molecules. The nanoscale marks the nebulous boundary between the classical and quantum mechanical worlds. Nanostructured materials have received steadily growing interests as peculiar and fascinating properties superior to their bulk counterparts.<sup>1</sup> Thus, realization of nanotechnology is promising to bring excellent capabilities and applications. Fabrication of nanomachines and nanodevices will undoubtedly solve an enormous amount of problems faced by mankind today.

So far, the carbon nanotubes (CNTs), Si nanowires (SiNWs) and other semiconductor nanowires such as GaN or ZnO nanowires etc. are successfully fabricated and widely studied.<sup>2-5</sup> CNTs have been applied in the fabrications of various devices such as scanning probes, biological sensors and electronic transistors etc. and the ZnO nanowire arrays are applied for nanolasers and nanogenerators.<sup>2</sup> Besides the porous materials are considered as the quasi one-dimensional (1D) structure that exhibits similar behaviors to nanowires such as blue shift photoluminescence (PL) and red shift in Raman scattering spectra due to the size confinement effects, and the surface phonon modes are observed in Raman spectrum. Therefore nanotechnology gives another opportunity for devices design and provides another field for fundamental researches, and it is possible to result in next industrial revolution.

## **1.2 Introduction to SnO<sub>2</sub> material**

SnO<sub>2</sub>, as an n-type wide-banded gap semiconductor ( $E_g = 3.6$  eV at 300 K for bulk SnO<sub>2</sub>) with rutile structure, exhibits interesting properties such as sensitivity to the environment, high chemical and thermodynamic stabilities.<sup>6</sup> Recently, attention has been focused on the research field of one-dimension (1D) nanostructures such as

wires and rods, because of both their fundamental properties and potential applications in nanodevices.<sup>7</sup> For example, in recent reports, SnO<sub>2</sub> nanowires (NWs) have been studied for field emission, electrochromic displays, and gas sensors.<sup>8,9</sup> Owing to the great sensitivity in ultraviolet (UV) region and conductance, SnO<sub>2</sub> NWs are also expansively applied in dye-based solar cells, transistors and transparent electrodes.<sup>10,11</sup> Although a considerable amount of researches have been performed on SnO<sub>2</sub> NWs, only relatively few experimental information about photoconductive characteristics in UV region has been reported.<sup>12</sup> Based on the remarkable photoconductance in UV region, SnO<sub>2</sub> NWs are promising for the fabrication of excellent visible-blind UV photodetectors



### **1.3 Photoconductivity**

The photoconductivity (PC) can be defined as the difference between the electrical conductivities under illumination and in the dark. Namely, PC is the change in resistance due to extra carriers from optical absorption in a semiconductor or in an insulator. It is concerned with optical excitation and transport phenomena. Light incident on the sample whose photon energy is bigger than the energy band gap of a semiconductor is absorbed with the effect, and additional electron-hole pairs are produced, resulting in an increase of conductivity.

PC offers a means of studying many physical properties of materials. Furthermore photoconductivity effects have obvious applications to the detection and measurement of light, in the whole spectrum. All these considerations explain why photoconductivity is a very useful subject.

The observation of any photoconductivity phenomenon requires the presence of at least one type of mobile charge carrier. If the conductivity due to these carriers is written as follows:

$$\sigma = q \mu n \tag{1.1}$$

where  $q$  is the magnitude of electronic charge,  $\mu$  is the mobility and  $n$  is the volumetric concentration, the photoconductivity, or variation of conductivity upon light irradiation, has the general form

$$\Delta \sigma = q(\mu \Delta n + n \Delta \mu). \tag{1.2}$$

Thus photoconductivity may arise due to a change in carrier concentration and/or carrier mobility. These changes result from the generation in the semiconductor of the electronic excited states by absorption of the light energy. Either these excited states represent the excess carrier concentration  $\Delta n$  or a mobility variation  $\Delta \mu$ , which is

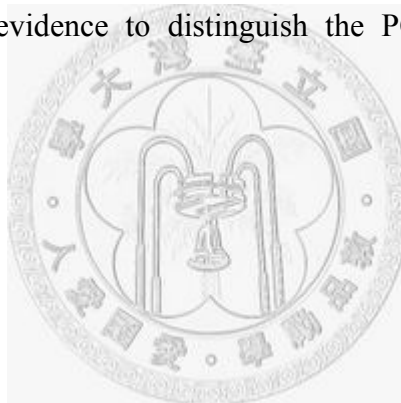
usually small enough to ignore. Therefore the PC is attributed to the  $\Delta n$ .

$$\Delta n = F\tau \quad (1.3)$$

is the fundamental relationship in the discussion of all photoelectronic phenomena, where  $F$  is the absorption rate of photon per sec and  $\tau$  is the lifetime of a free carrier. The lifetime  $\tau$  is usually a function of  $F$ , so the equation can be expressed as

$$\Delta n \propto F^{1-\kappa} . \quad (1.4)$$

The value of  $\kappa$  is the evidence to distinguish the PC mechanism and will be discussed later.





## References

1. Y. Xin, P. Yang, Y. Sun, Y. Wu, B. MAyers. B. Gates, Y.Yin, F. Kim, and H. Yan, Adv. Mater. (Weinheim, Ger.) **15**, 353(2003).
2. S. Iijima, Nature **354**, 56 (1991).
3. D. P. Yu, Z. G. Bai, S. Q. Feng, C. S. Lee, I. Bello, X. S. Sun, Y. H. Ang, G. W. Zhou, Z. Zhang, Solid State Commun. **105**, 403 (1998).
4. H. Morkoc, S. N. Mohammad, Science **267**, 51 (1995).
5. E. J. Lerner, Ind. Phys. **7**, 10 (2001).
6. S. Luo, P. K. Chu, W. Liu, M. Zhang, and C. Lin, Appl. Phys. Lett. **88**, 183112 (2006)
7. B. Wang, Y. H. Yang, C. X. Wang, and G. W. Yang, J. Appl. Phys. **98**, 124303 (2005).
8. B. Wang, Y. H. Yang, C. X. Wang, and G. W. Yanga, J. Appl. Phys. **98**, 073520 (2005).
9. F. Hernandez-Ramirez, S. Barth, A. Tarancon, O. Casals, E. Pellicer, J. Rodriguez, A. Romano- Rodriguez, J. R. Morante, and S. Mathur, Nanotechnology, **18**, 424016 (2007).
10. G. Vilaca, B. Jousseume, C. Mahieux, C, Belin, H. Cachet, M. Bernard, V. Vivier, and T. Toupance, Adv. Mater. (Weinheim, Ger.) **18**, 1073 (2006).

11. R. Liu, Y. Chen, F. Wang, L. Cao, A. Pan, G. Yang, T. Wang, and B. Zou, *Physica E*, **39**, 223 (2007).

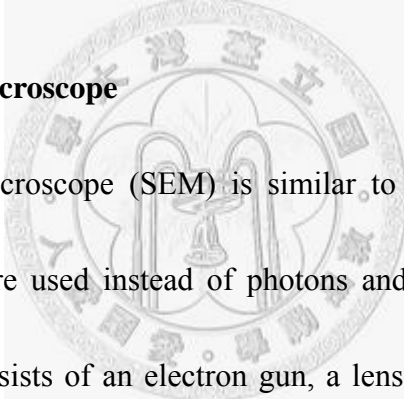
12. Z. Liu, D. Zhang, S. Han, C. Li, T. Tang, W. Jin, X. Liu, B. Lei, and C. Zhou, *Adv. Mater. (Weinheim, Ger.)* **15**, 20 (2003).



## Chapter 2

### Experimental instruments and details

#### 2-1 Scanning Electron Microscope

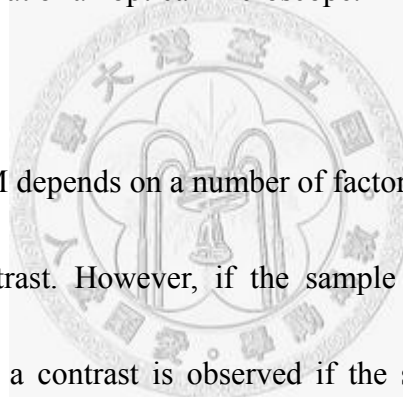


Scanning electron microscope (SEM) is similar to light microscope with the exception that electrons are used instead of photons and the image is formed in a different way. A SEM consists of an electron gun, a lens system, scanning coils, an electron collector, and a liquid crystal display (LCD). An electron beam is utilized to produce a magnified image of a sample in electron microscope. The electron energy is typically 10-30 KeV for most samples, but for insulating samples, the energy could be as low as several hundred eV. The utilization of electrons has two main advantages over typical microscopes. Much larger magnifications are possible since electron wavelength are much smaller than the photon wavelengths and the depth of field is much higher.

De Broglie proposed in 1923 that particles can also behave as waves. The electron wavelength  $\lambda_e$  depends on the dynamics energy or the accelerating voltage  $V$  as

$$\lambda_e = \frac{h}{\sqrt{2mE_k}} = \frac{h}{\sqrt{2mqV}} = \frac{1.22}{\sqrt{V}} \text{ (nm)} \quad (2.1)$$

The wavelength is 0.012 nm for  $V=10000$  V which is significantly smaller than the wavelength in visible range (400 nm~700 nm). Consequently, The resolution of an SEM is much better than that of an optical microscope.

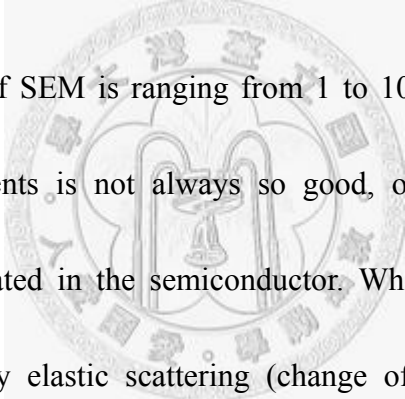


The contrast in a SEM depends on a number of factors. For a flat uniform sample, the image shows on contrast. However, if the sample consists of materials with different atomic numbers, a contrast is observed if the signal is obtained from the backscattered electrons, because the backscattering coefficient increases with the atomic numbers  $Z$ . Nevertheless, the secondary electron emission coefficient is not a strong function of  $Z$  and atomic number variations give no appreciable contrast. Contrast is also influenced by the surface conditions and by the local electric field. But the main contrast-enhancing feature is the sample topography. Secondary electrons are emitted form the top 10 nm or so of the sample surface. When the sample surfaces is tilted from the normal beam incidence, the electron beam path

lying within this 10nm is increase by the factor  $\frac{1}{\cos\theta}$  where  $\theta$  is the angle from the normal incidence ( $\theta = 0^\circ$  for normal incidence). The interaction of the incident beam with the sample increases with path length and the secondary electron emission coefficient increases. The contrast C depends on the angle as

$$C = \tan(\theta)d\theta \quad (2.2)$$

For  $\theta = 45^\circ$ , a change in the angle of  $d\theta = 1^\circ$  produces a contrast of 1.75% while at  $60^\circ$  the contrast increases to 3% for  $d\theta = 1^\circ$ .



The beam diameter of SEM is ranging from 1 to 10 nm. Yet the resolution of electron beam measurements is not always so good, owing to the shape of the electron-hole cloud generated in the semiconductor. When electrons impinge on a solid, they lose energy by elastic scattering (change of direction with negligible energy loss) and inelastic scattering (energy loss with negligible change in direction). Elastic scattering is caused mainly by interactions of electrons with nuclei and is more probable in high atomic number materials or at low beam energies. Inelastic scattering is caused mainly by scattering from valence and core electrons. The result of these scattering events is a broadening of the original nearly collimated, well-focused electron beam within the sample.

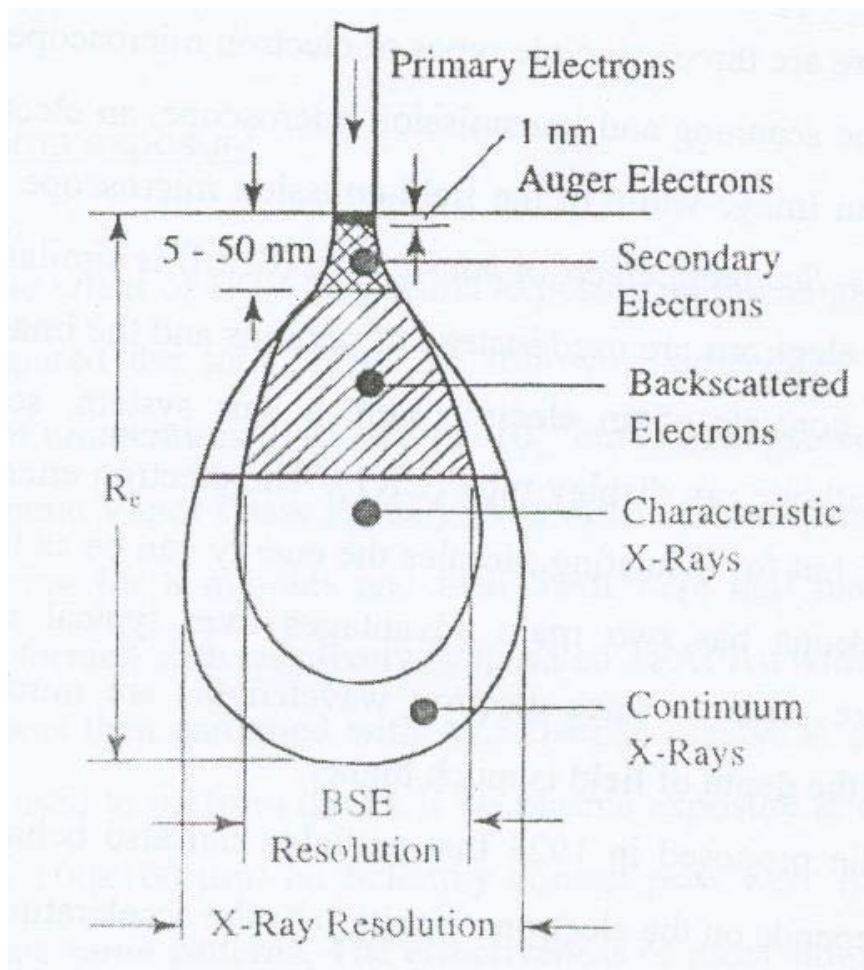


Fig. 2-1: Summary of the range of and spatial resolution of backscattered electrons, secondary electrons, X-ray, and Auger electrons for electrons incident on a solid, and etching the exposed portion of the materials. Electron trajectories, calculated with Monte Carlo techniques, also agree with these shapes.

The generation volume is a function of the electron beam energy and the atomic number  $Z$  of the sample. Secondary electrons, backscattered electrons, characteristic and continuum X-rays, Auger electrons, photons, and electron-hole pairs are produced.

For low- $Z$  samples there is considerable scattering near the surface and a large fraction of the incident electrons is backscattered. The shape of the electron distribution is teardrop-shaped as shown in Fig. As  $Z$  increases ( $15 < Z < 40$ ) the shape becomes more spherical and for  $Z > 40$  it becomes hemispherical. "Teardrop" shape has been observed by exposing polymethylmethacrylate to an electron beam.

The depth of electron penetration is the electron range  $R_e$ , defined as the average distance from the sample surface where an electron travels. A number of empirical expressions have been derived for  $R_e$ . Once such expression is

$$R_e = \frac{4.28 \times 10^{-6} E^{1.75}}{\rho} \text{ (cm)}, \quad (2.3)$$

where  $\rho$  is the density ( $\text{g/cm}^3$ ) of the sample and  $E$  is the electron energy (KeV).

## 2-2 X-ray Diffraction

The crystalline structure can be analyzed by X-ray diffraction using the Bragg equation:

$$2d \sin \theta = n\lambda \quad (2.4)$$

where  $d$  is the distance between the crystal planes,  $\lambda$  is the wavelength of X-ray, and Cu K $\alpha$  line is used here.  $\theta$  is the Bragg diffraction angle. As illustrated in Fig. 2-2, the incident angle and diffraction angle are scanned simultaneously in  $\theta$ - $2\theta$

XRD.  $\theta$ - $2\theta$  XRD is used to analyze the crystal planes parallel to the substrate surface. According to equation 2.4, the diffraction peaks in the  $\theta$ - $2\theta$  XRD patterns could be used to determine the  $d$  values, and then to identify the orientation of the films

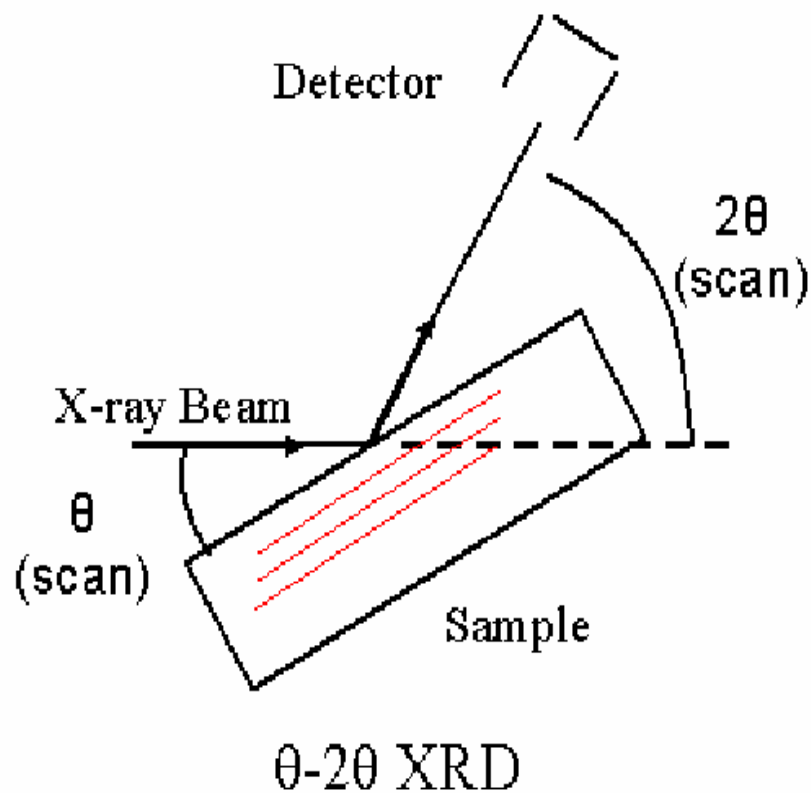


Fig. 2-2: The X-Ray Apparatus

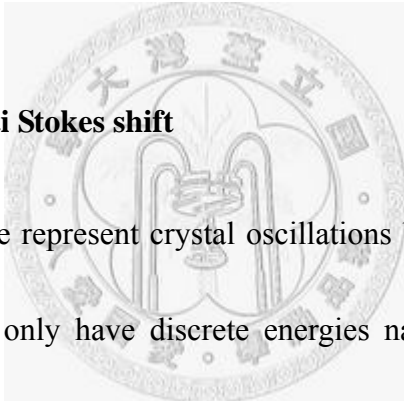
### 2-3 Raman Scattering

Raman scattering effect is an inelastic scattering phenomenon of light with materials. Indian physicist, C.V. Raman, first observed this effect in 1928. It involves a change in photon frequency. When the photons encounter the surface of a



semiconductor, they will mostly be reflected, transmitted, absorbed, or Rayleigh scattered, because of first-order elastic interaction with electrons, phonons, and impurities. There is no change in photon frequency during these elastic interactions. However, a small fraction of the light interacts inelastically with phonon modes producing outgoing photons whose frequencies are shifted from the incoming values. These are the Raman-scattered photons. This interaction of incident light with optical phonon is called Raman scattering.

### **2-3-1 Stokes shift and Anti Stokes shift**



In quantum theory, we represent crystal oscillations by supposing some quanta, so-called phonons, which only have discrete energies named energy levels. When light incident into a semiconductor interacting with crystal oscillations, we can view this situation as photon interacting with phonon which is possibly at different energy level. Consider phonons at ground state ( $n=0$ ) and first excited state ( $n=1$ ) with interval of  $h\omega$ . As a photon (with frequency  $\nu$ ) interacts with a phonon at first excited state, the phonon absorbs its energy exciting to a higher energy level with energy  $h(\nu + \omega)$ . Due to the short lifetime (about  $10^{-4}$  sec) of this higher energy state, the phonon will soon fall down to a lower energy state. If it goes back to the ground state, an anti-Stokes photon will be released in this process. If the phonon goes back to the first

excited state, a Rayleigh-scattered photon will be produced. Similarly, a photon interacting with a phonon at ground state will excite the phonon to a higher level of  $h\nu$ . A Rayleigh-scattered photon (see Fig. 2-3-1) will be produced as the phonon decays to the ground state. A Stokes photon will be produced as the phonon decays to the first excited state.

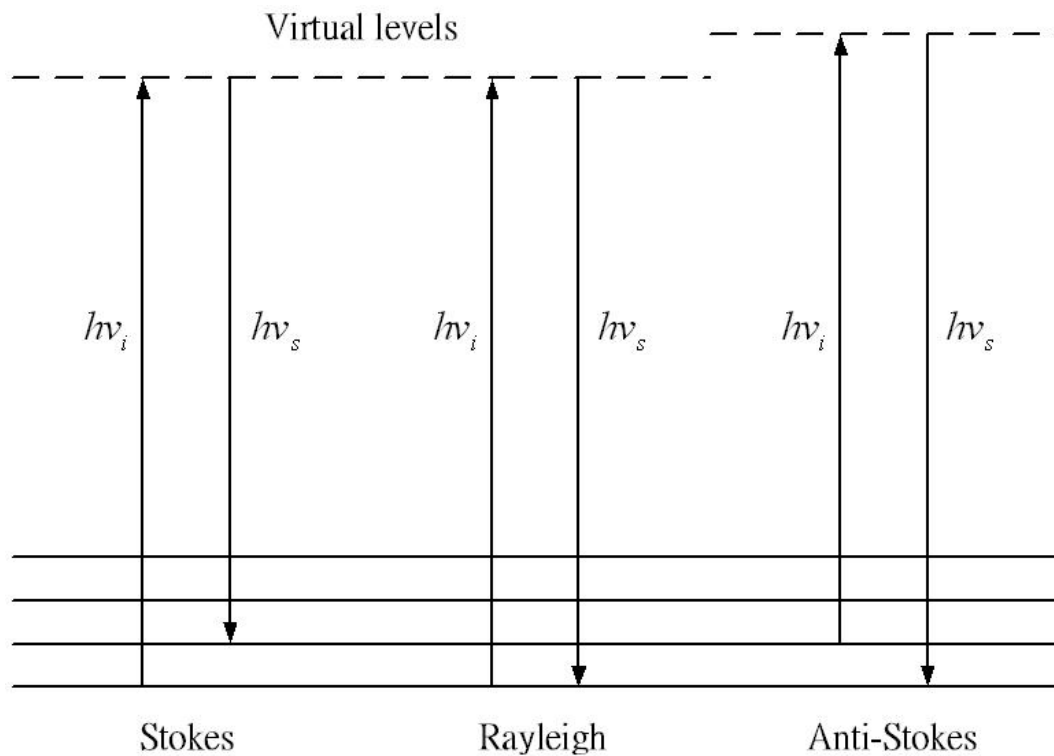


Fig 2-3-1: Ideal model of Stokes and Anti-Stokes Raman scattering.

As described above, those Raman-scattered photons gain energy by absorbing a phonon (anti-Stokes shifted), or lose energy by emitting one (Stokes shifted). Both of

the processes must obey the energy and momentum conservation rules. The conservation conditions can be written as:

$$h\nu_s = h\nu_i \pm h\omega, \quad (2.5)$$

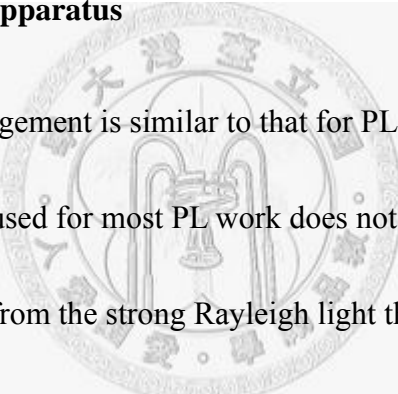
$$\mathbf{k}_s = \mathbf{k}_i \pm \mathbf{k}_0, \quad (2.6)$$

where  $\nu_i$  and  $\nu_s$  are the incoming and scattered photon frequencies respectively,  $\mathbf{k}_i$  and  $\mathbf{k}_s$  are the incoming and scattered photon wave vectors respectively, while  $\omega$  and  $\mathbf{k}_0$  are the phonon frequency and wave vector respectively. The values of frequency shift resulting from Raman scattering range from ten to a few thousand  $\text{cm}^{-1}$ . Normally speaking, the intensity of the Stokes component is much stronger than that of the anti-Stokes line because usually there are few phonons to be absorbed compared to the number of phonon that can be emitted. Raman scattering is inherently a weak process, but lasers provide enough power so that the spectra can be routinely measured. One thing needs to be emphasized is that those Raman shifts measured are precisely the frequencies of crystal oscillations regardless of the frequency of incident light.

However, a change in the wavelength of the exciting radiation changes the penetration, giving flexibility in the probe depth. The small wavelength of exciting

radiation, combined with Raman microprobe techniques, also provides good spatial resolution<sup>3</sup>. Owing to the close relation between Raman scattering and the oscillations of atoms and molecules inside the materials, we can gain the information about the oscillations of atoms and molecules inside the materials from Raman scattering spectrum. These oscillations are mainly controlled by interatomic or intermolecular interactions. Raman-scattering researches can therefore provide a way for people to understand these interaction force.

### **2-3-2 Raman Scattering Apparatus**



A typical Raman arrangement is similar to that for PL with one major difference: the single monochromator used for most PL work does not discriminate sufficiently to separate the Raman signal from the strong Rayleigh light that accompanies it. The double monochromator is needed in order to increase discrimination, which consists of two ganged gratings turning together and sequentially selecting the light. In some case, for instance to examine Raman peaks with a few wavenumbers of the exciting line, triple monochromator must be used. Besides, the Raman system may also include means to polarize the exciting light and analyze the polarization of the scattered light. These polarization states are intimately connected to the orientation of a crystalline sample.

Our Raman scattering system is arranged as in Fig. 2-3-2 and the laser light source is Ar<sup>+</sup> laser (working at 514.5 nm). Raman spectrometer is the

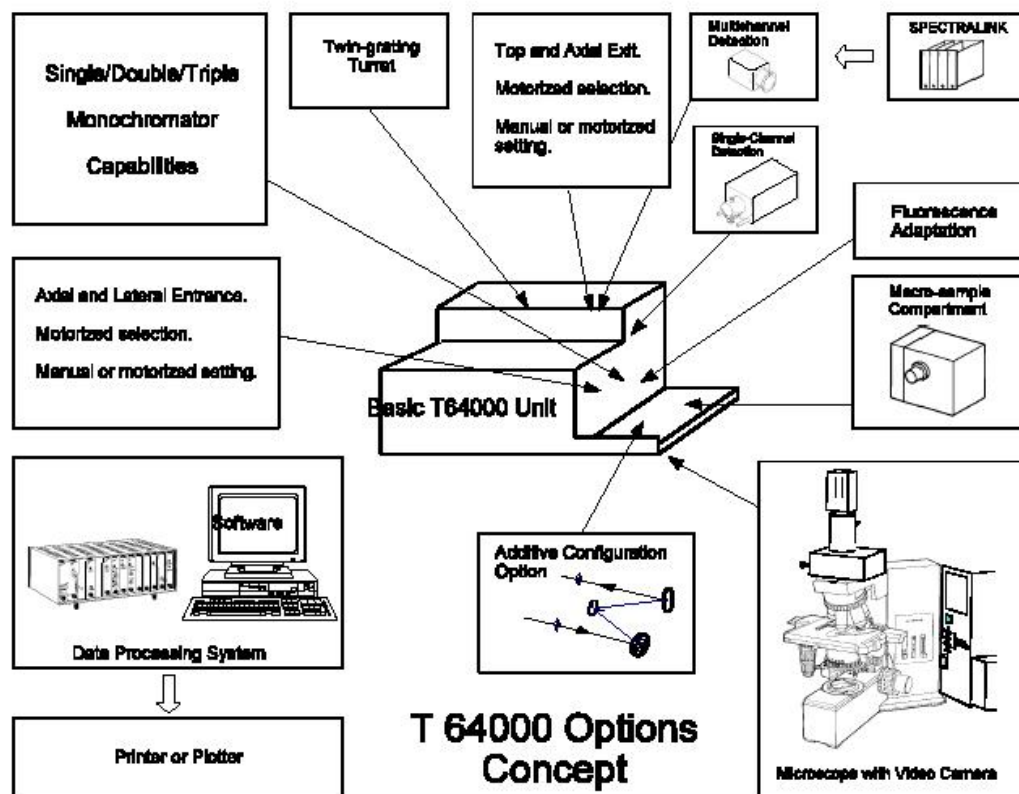


Fig. 2-3-2 Jobin-Yvon T64000 Micro-Raman System.

T64000 micro-Raman system that produced by the Jobin-Yvon Company. After going through a half-wave plate, the incident laser light is focused on the sample. The scattering lights collected by a lens are focused on the slit of the spectrometer. As

shown in Fig. 2-3-3, the optics can be arranged so that the Raman scattered light is coupled to the monochromator through the microscope, and auxiliary illuminating light is sent to a video camera to give a real-time images of the sample surface. This makes it possible to locate and probe areas of the sample as small as the bean size.

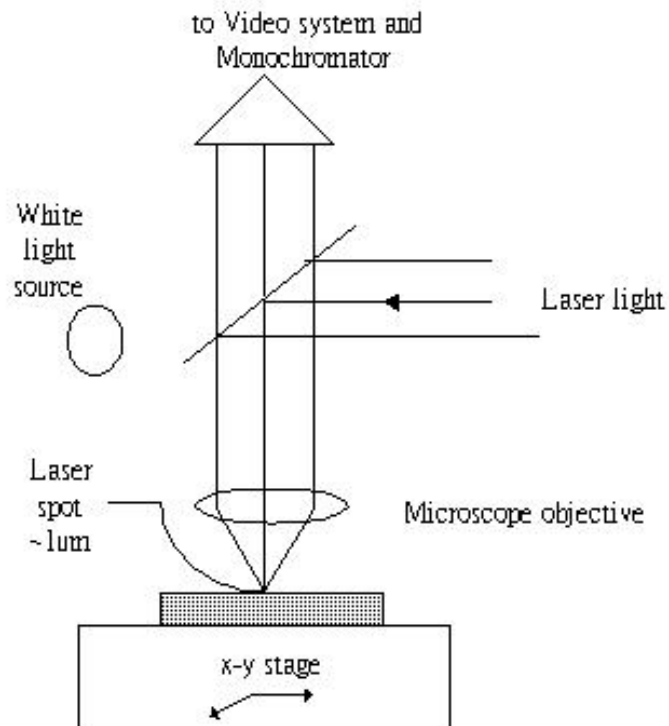


Fig. 2-3-3: Schematic of a Raman microscope. The microscope objective lens focuses the laser beam to a spot size of about  $1 \mu\text{m}$ . Scattered light is transmitted through the beam splitter to the triple monochromator, giving the Raman spectrum of the selected region. Visible light from the illuminator is reflected from the sample to a video camera, giving a realtime image to the

allow position of the probe beam. The sample can be moved on the x-y stage.

## **2-4 Experimental details and setups**

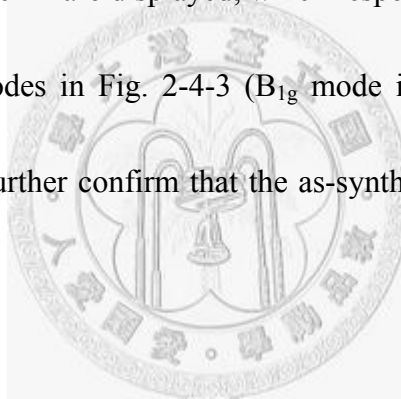
Here, we will particularly report our experimental details and setups. First we will illustrate the synthesizing method of SnO<sub>2</sub> NWs. Fabrication of a single nanowire device on sapphire will also be reported in subsequent sections. In addition, the method that we proceed in photoconductivity and Au-decoration will be illustrated.

### **2-4-1 Synthesis of SnO<sub>2</sub> nanowires**

The growth of SnO<sub>2</sub> NWs is based on the method named vapor-liquid-solid (VLS). In the synthesizing process, the Au layer (about 10 nm in thickness) is first deposited on M-plane (100) sapphire (Al<sub>2</sub>O<sub>3</sub>). Then Sn powder is placed on the ceramic boat and put into a furnace with Argon flow as gas carriers at the flow rate 200 sccm. The temperature is rapidly increased from room temperature up to 1000 °C by a rate of about 100 °C/min and Sn vapor is mixed with oxygen in air and turns into SnO<sub>2</sub> and blown onto the Au catalyst. After SnO<sub>2</sub> dissolves into Au, the supersaturation of the alloy SnO<sub>2</sub>-Au droplet results in the nucleation, and SnO<sub>2</sub> NWs are fabricated. The as-grown SnO<sub>2</sub> NWs have a diameter of 100~300 nm and length above 40 μm as shown in Fig. 2-4-1. In Fig. 2-4-2(a), the XRD graph is employed to

identify the structure of synthesized products. Most of the peaks are perfectly indexed according to the tetragonal rutile structure of SnO<sub>2</sub>.

Rutile SnO<sub>2</sub> belongs to the space group  $D_{4h}^{14}$  of which the normal lattice vibration at the  $\Gamma$  point of the Brillouin zone is given on the basis of group theory:  $\Gamma = 1A_{1g} + 1A_{2g} + 1A_{2u} + 1B_{1g} + 1B_{2g} + 2B_{1u} + 1E_g + 3E_u$ . Among them, the four first order active Raman modes are B<sub>1g</sub>, E<sub>g</sub>, A<sub>1g</sub>, and B<sub>2g</sub>. In Fig. 2-4-2(b), the three Raman peaks at 478, 637, and 779cm<sup>-1</sup> are displayed, which respectively correspond to the E<sub>g</sub>, A<sub>1g</sub>, and B<sub>2g</sub> vibration modes in Fig. 2-4-3 (B<sub>1g</sub> mode is at the 123cm<sup>-1</sup> not shown here). Thus, these peaks further confirm that the as-synthesized SnO<sub>2</sub> NWs have the tetragonal rutile structure.



If we replace Au catalyst layer with Ti, the different fabrications can be formed. The SEM graph shows the products, and the nanobelts are synthesized. The width is ranging from 100 nm to 1  $\mu$  m as shown in Fig. 2-4-4.

#### **2-4-2 Fabrication of SnO<sub>2</sub> nanowires device**

The SnO<sub>2</sub> NWs were removed from the M-plane sapphire by percussion and transferred to another clean sapphire as an insulator. Using a simple commercially



available copper grid as a shadow-mask method with square openings of  $100 \times 100 \mu\text{m}^2$  and spacing  $10 \mu\text{m}$ , the ends of the wires were contacted by vacuum thermal evaporation, and Ni/Au (15/150 nm thickness) electrodes for SnO<sub>2</sub> to achieve Ohmic contacts. Figure 2-4-5 shows SEM image of the SnO<sub>2</sub> NWs contacted at both ends by the Ni/Au pads.

### **2-4-3 Two terminal I-V measurement**

The two terminal  $I$ - $V$  (current versus voltage) curve is measured by the system of two probes, Keithley-4200 electrometer and optical electron microscope. A single SnO<sub>2</sub> NW device is put down in the holder under microscope. Two probes contact between the Ni/Au contact which a single wire strides across both side. When we ensure that two probes are contacted perfectly, we use Keithley-4200 system to supply bias on the SnO<sub>2</sub> NWs device to measure  $I$ - $V$  relation and record it.

### **2-4-4 Photoconductivity measurement in air and in vacuum**

In our photoconductivity experiment, we use He-Cd laser whose photon energy (3.81 eV) is larger than the energy band gap of SnO<sub>2</sub> (3.6 eV). The powermeter is used to measure the light power spotted on the device. By measuring the current without 325 nm UV illumination and current with 325 nm UV illumination, we can

calculate the generated-photocurrent by subtracting these two currents.

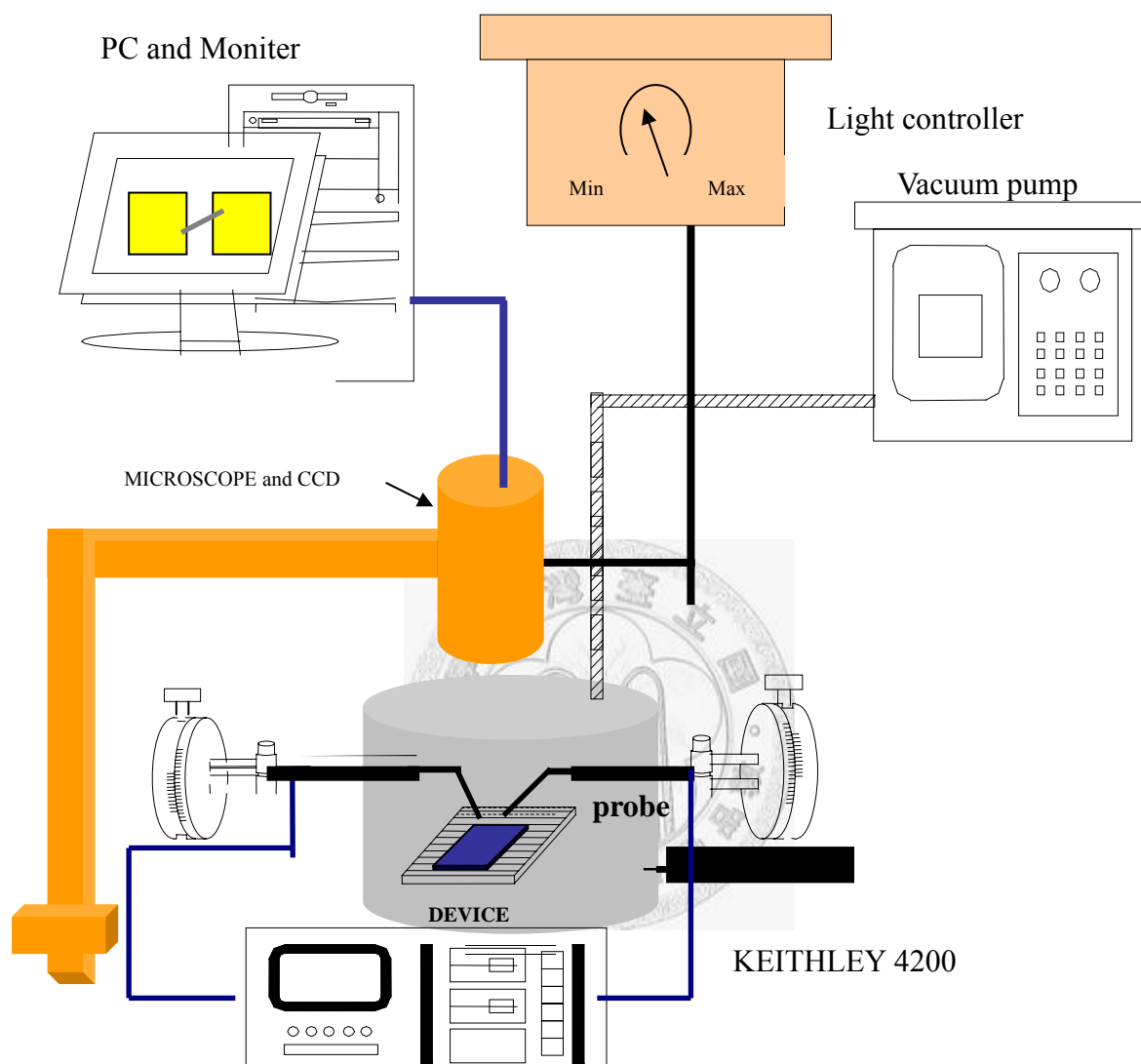


Fig. 2-4: The setup of air and vacuum measurement system.

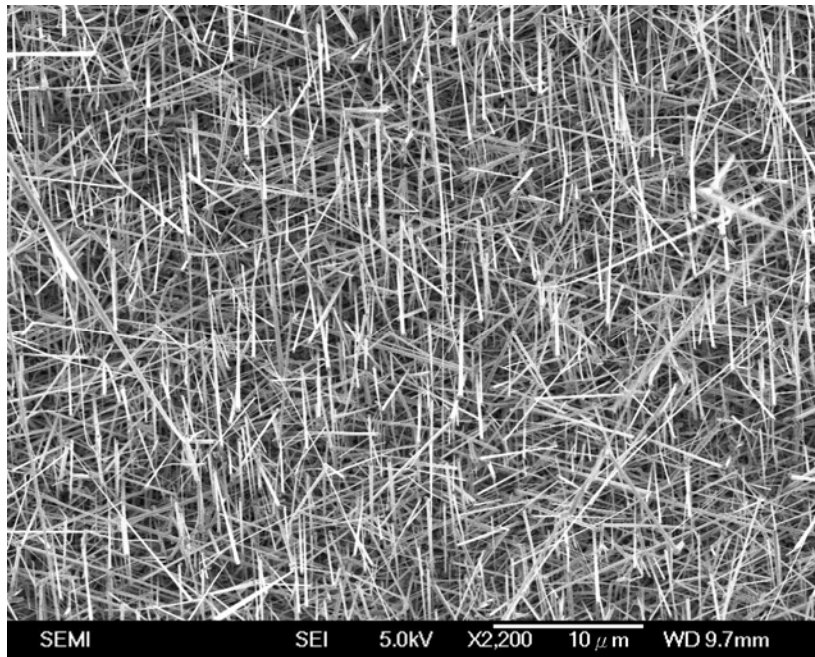
## 2-5 Sputtering metallic nanoparticles

After the SnO<sub>2</sub> NWs device is set in the chamber, the ambient pressure is pumped below 10 Pa readily, and then the JFC coater sputters the metallic

nanoparticles out. The sputtered Au-nanoparticles are consequently dropped at the surface of SnO<sub>2</sub> NW uniformly and the random distribution as shown in Fig 2-5. The distribution density is low enough that the screen effect on SnO<sub>2</sub> NWs will not happen. Additionally, the Au-nanoparticles do not construct a new conductive path on the substrate to influence the PC measurement.



(a)



(b)

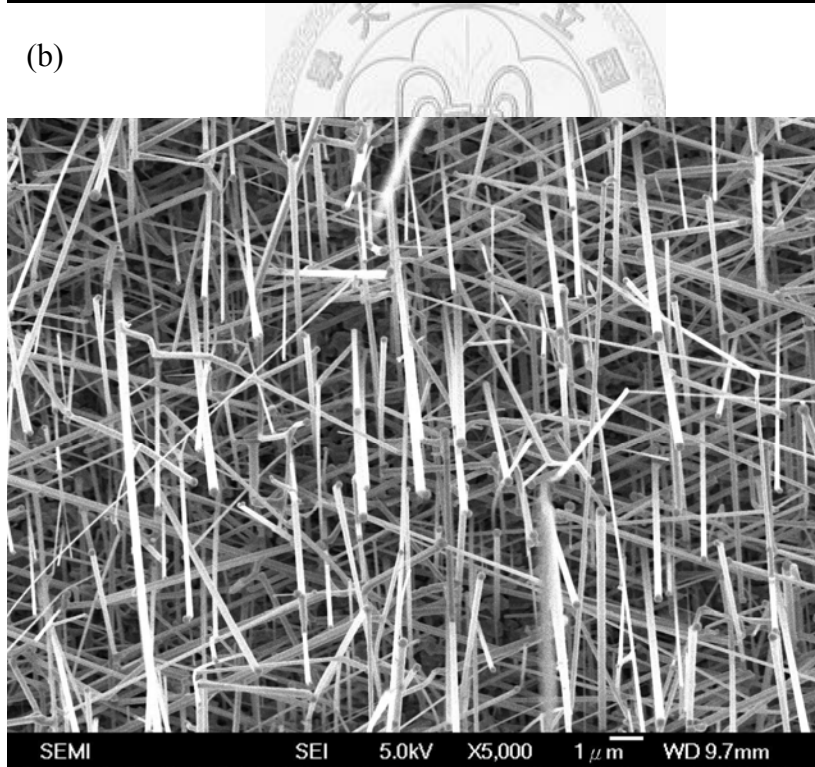
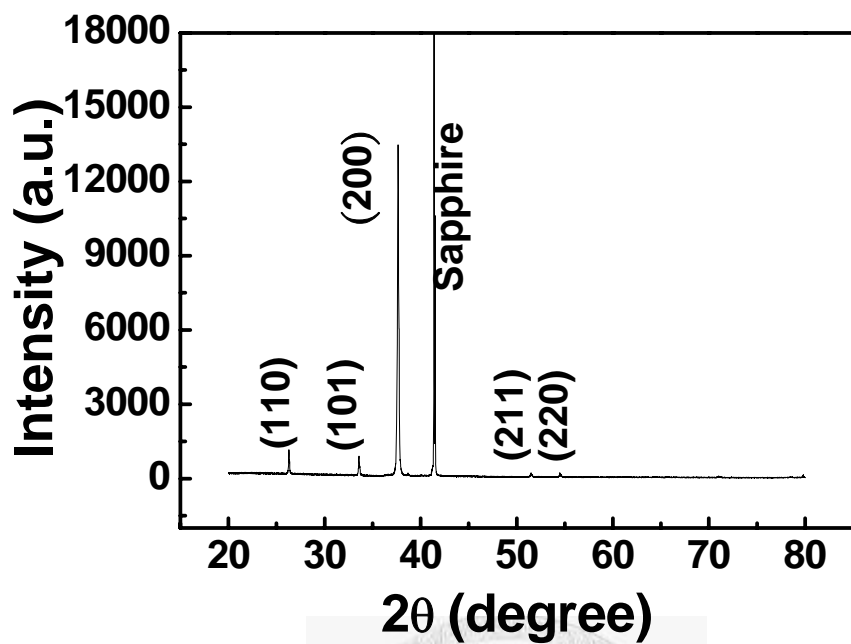


Fig. 2-4-1: (a)(b) Scanning electron microscope image of SnO<sub>2</sub> NWs deposited on

M-plane sapphire.

(a)



(b)

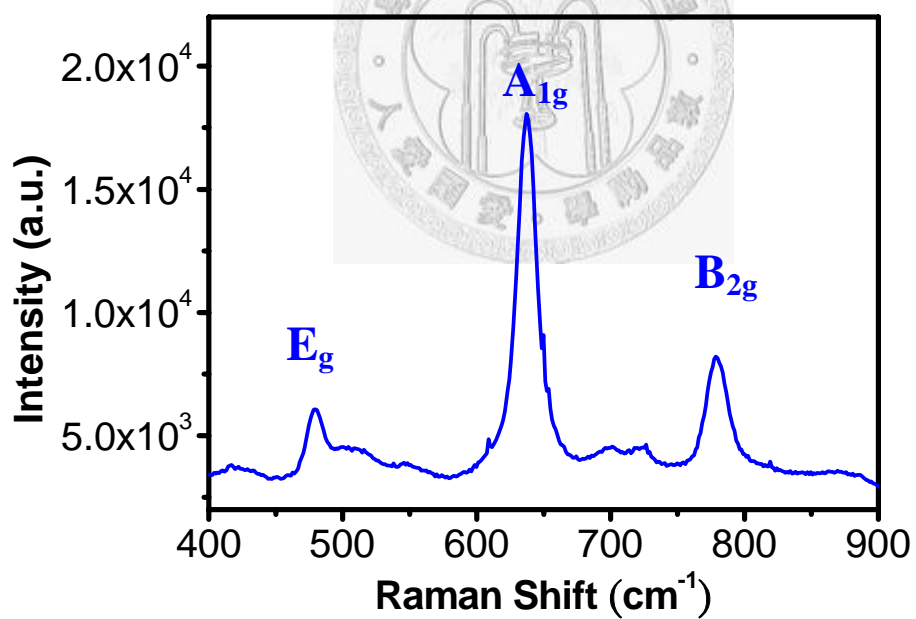


Fig. 2-4-2: The corresponding (a) X-ray diffraction pattern and (b) Raman spectrum measured from the as-synthesized SnO<sub>2</sub> nanowires.

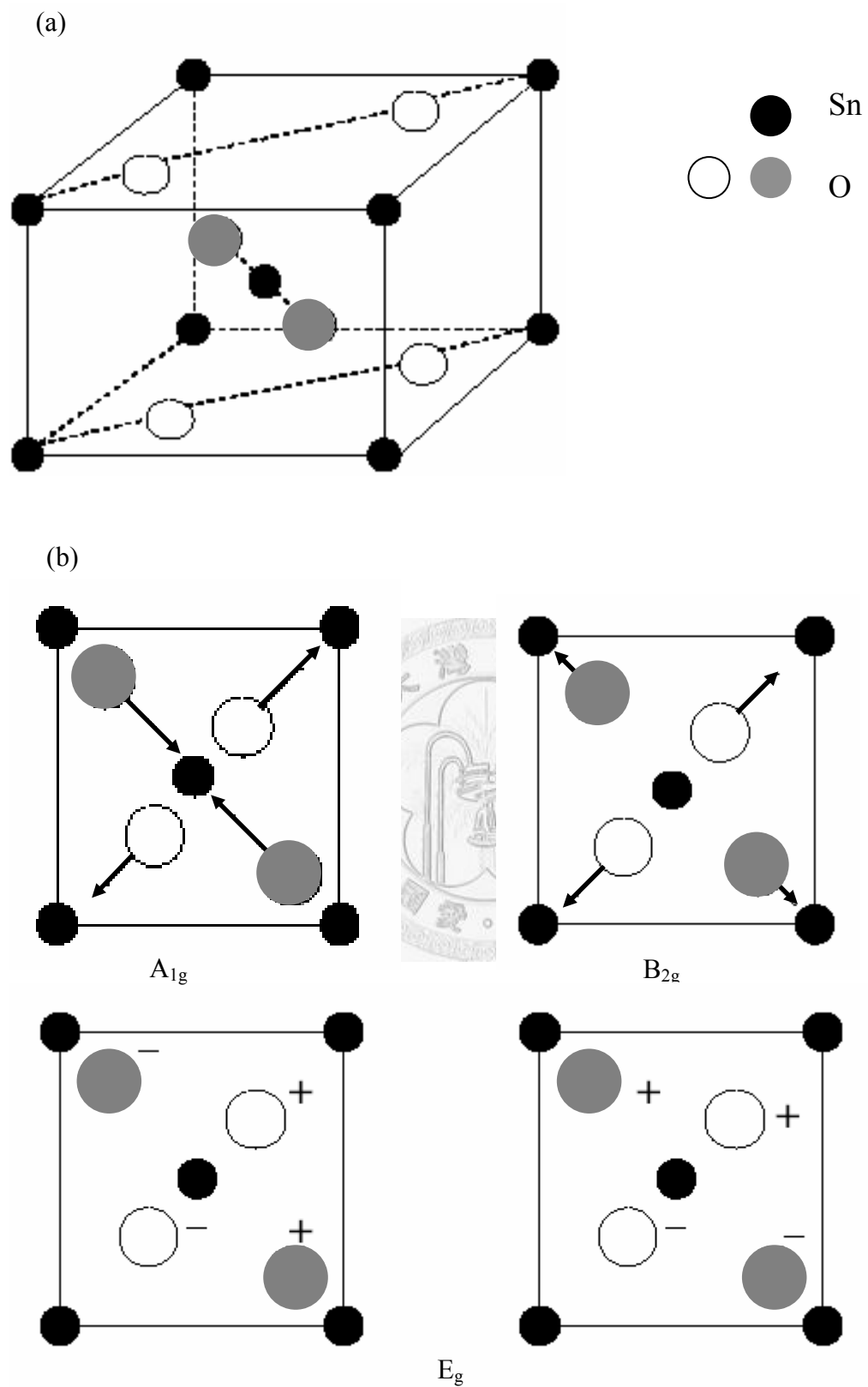
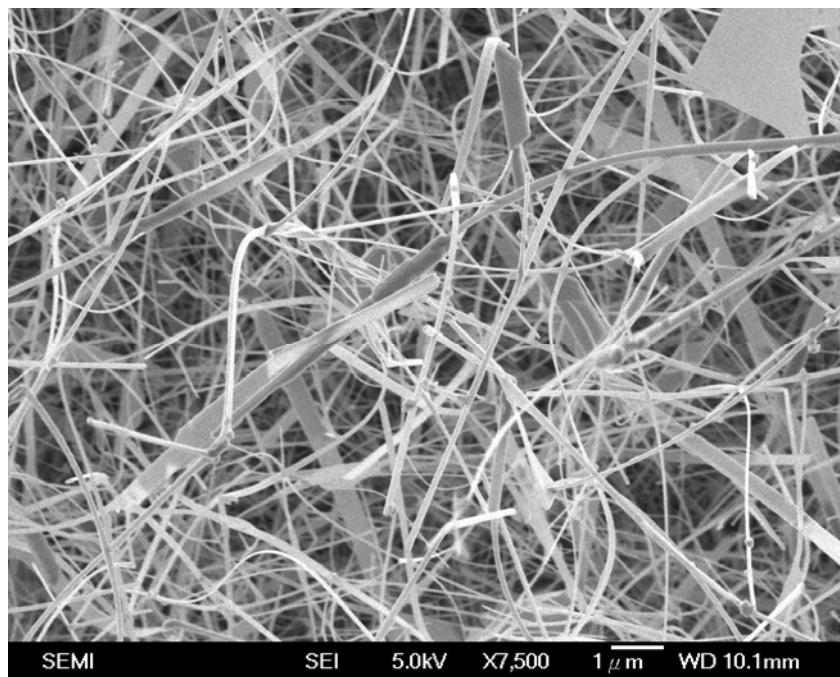


Fig. 2-4-3 (a) Unit cell of the structure of  $\text{SnO}_2$ . (b) Atomic displacement of atoms, viewed along the  $c$  axis, associated with Raman-active modes.

(a)



(b)

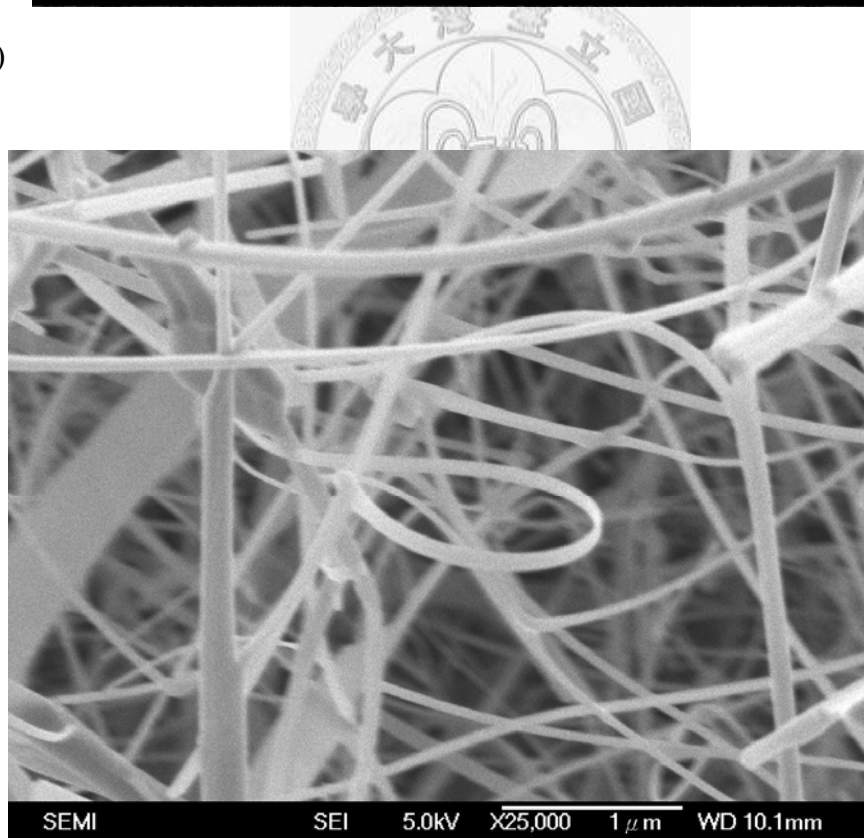


Fig. 2-4-4: (a)(b) Various magnifying scanning electron microscope patterns of the morphologies of the fabricated SnO<sub>2</sub> nanobelts

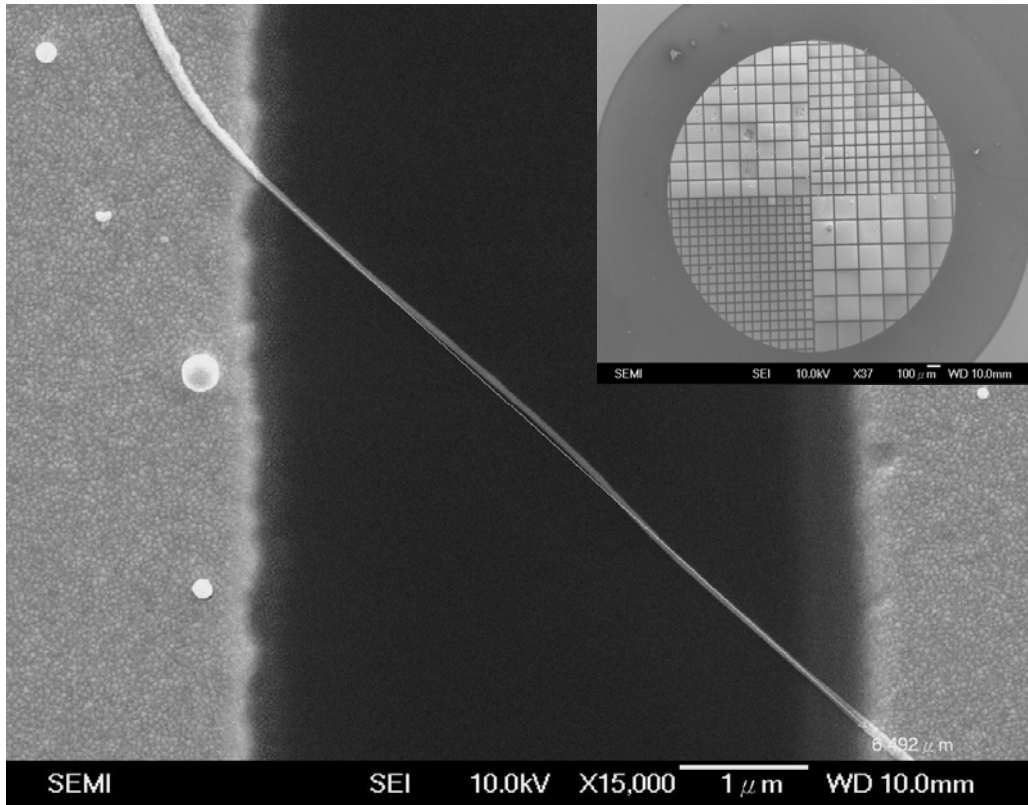


Fig 2-4-5: Scanning electron microscope image of a single SnO<sub>2</sub> nanowire straddled with Ni/Au pad and the plug by the shadow mask method.



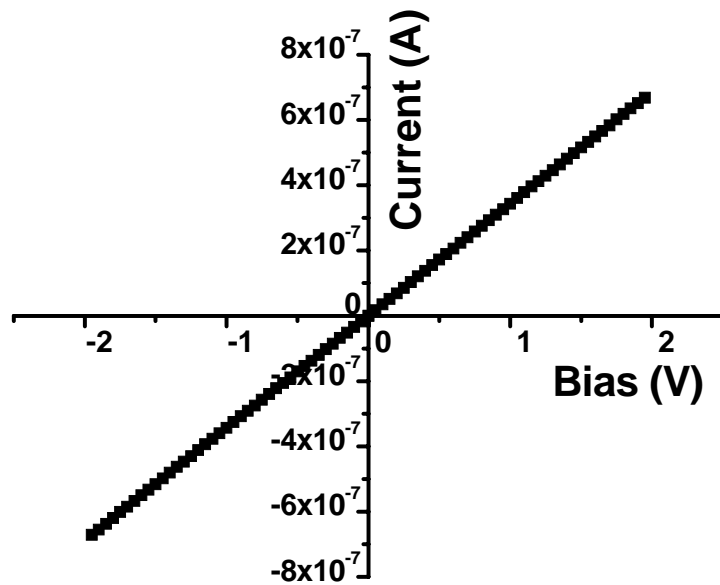


Fig. 2-4-6: The SnO<sub>2</sub> Nanowire between two terminals exhibits perfect Ohmic characteristics.

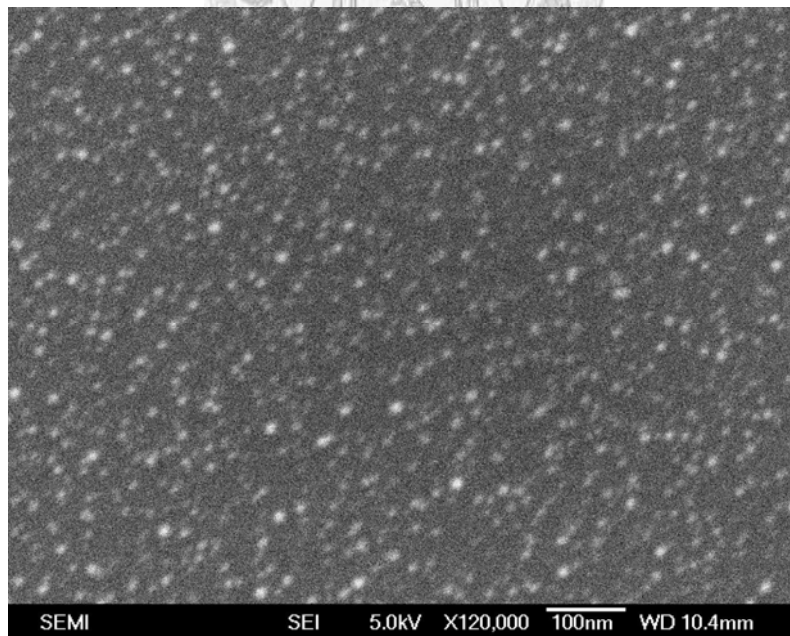
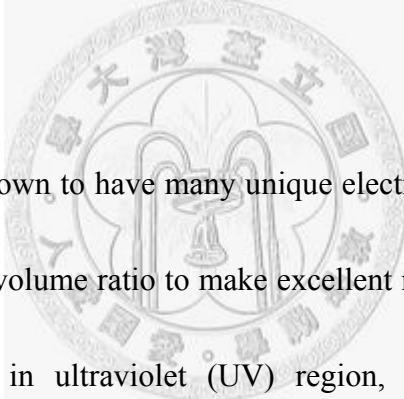


Fig 2-5: Au-nanoparticles random distribution on the Si substate.

## Chapter 3

### High photocurrent gain in SnO<sub>2</sub> nanowires

#### 3-1 Introduction



1D SnO<sub>2</sub> NWs are known to have many unique electronic and optical properties due to the high surface-to-volume ratio to make excellent nanodevices. Because of its high quantum efficiency in ultraviolet (UV) region, it is extensively used in visible-blind photodetectors.<sup>6</sup> Additionally, SnO<sub>2</sub> thin films and NWs have also been used in active pollutant gas sensors based on the measurement of resistance, such as H<sub>2</sub>, CO, and NO<sub>2</sub> etc.<sup>7-9</sup> For both, the most quoted model to explain the resistance change is that the adsorbed oxygen on the surface will extract the electron from semiconductor metal oxide, and react with chemical gas, and then the conductivity is altered. Even this premise has been adapted to explain the photoresponse of metal oxides, such as ZnO and SnO<sub>2</sub>;<sup>10,11</sup> however, so far, a quantitative description of the

photoresponse gain of SnO<sub>2</sub> NWs is still lacking, and the underneath mechanism of the photoresponse has not been well established. In this letter, we point out that the mechanism responsible for the photocurrent (PC) in SnO<sub>2</sub> NWs includes oxygen-related hole-trap states at the surface of NW as well as band-bending induced by surface electric field.

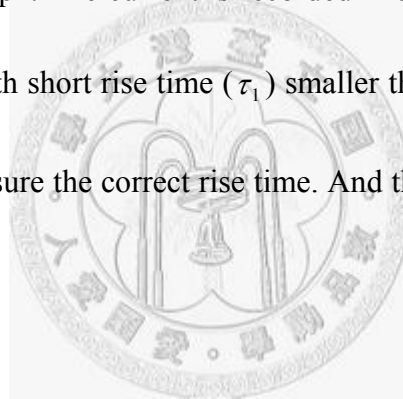
### 3-2 Results and Discussion

SnO<sub>2</sub> is a direct band-gap semiconductor with good optical adsorption in UV region as shown in Fig. 3-1. On illumination with photon energy larger than the energy band gap (~3.6 eV), the conductivity of the sample increases drastically due to photoexcited electron-hole pairs. Figure 3-2 shows the current of the sample with a bias of 0.1 V and under the illumination of a He-Cd laser working at 325 nm with different excitation intensity. The gain ( $\Gamma$ ) of the photoresponse could be obtained by expression,<sup>13</sup>

$$\Gamma = \frac{\Delta i / q}{P / h\nu}, \quad (3.1)$$

where  $\Delta i$  is the current difference between photocurrent and dark current,  $q$  is the electron charge,  $h\nu$  is the photon energy of incident light,  $P$  is the power of photon that the NW has absorbed, which means  $P = I \times l \times d$ .  $I$  is the exciting intensity illuminating the pattern,  $l$  and  $d$  are the length and the width of the NW,

respectively.  $\eta$  is the quantum efficiency which is set to be 1 for simplicity. Quite surprisingly, the calculated gain for the SnO<sub>2</sub> NW can be as high as 8000, which implies that SnO<sub>2</sub> NWs can serve as a highly sensitive photodetector. It will be very interesting to understand the mechanism behind the large photoresponse gain. According to the reports of Binet et al and Muñoz et al,<sup>14,15</sup> the relation between the gain and the illumination intensity is very useful to reveal the mechanism responsible for photocurrent. There are 2 types of PC can be observed with “short rise time” and “long rise time” in the graph. The current is recorded in an interval of 0.5 s, and can still measure a step PC with short rise time ( $\tau_1$ ) smaller than 0.5 s (even smaller than 0.01 s), so we cannot measure the correct rise time. And the focus is on the “long rise time” PC.



As shown in Fig. 3-3(a), for the excitation intensity below the critical value of 2 W/m<sup>2</sup>,  $\Gamma$  does not depend on the intensity, which means  $\Gamma$  remains constant. This behavior can be understood in term of oxygen-related hole-trap states at the surface of NW.<sup>14,16</sup> When SnO<sub>2</sub> NWs are exposed in air and adsorb oxygen molecules at their surface, the adsorbed oxygen molecules will capture electrons from the NWs and become negatively charged.<sup>16</sup> It can be described by the expression



After the UV light illumination, the photoinduced holes will migrate to the surface by the surface electric field and discharge negative-charged oxygen molecules, as described the expression,<sup>16</sup>



Accordingly, the neutralized oxygen molecules are photodesorbed from the surface . Therefore, the presence of hole-trap states prolongs the photoinduced electron lifetime, and hence the large value of gain can be understood. Indeed,  $\Gamma$  is defined as  $\tau\mu\Phi/l^2$ , where  $\tau$  is the carrier lifetime,  $\mu$  is the carrier mobility,  $\Phi$  is applied voltage. When the excitation intensity is low,  $\tau$  remains unchanged. Therefore,  $\Gamma$  does not depend on the excitation intensity. The oxygen-related hole-trap mechanism results in photoconductive gain as high as  $10^4$ . Nevertheless, once the excitation intensity exceeding the critical intensity ( $2 \text{ W/m}^2$ ), oxygen-related hole-trap states will be filled and change the electron-hole recombination behavior, and then lower down the gain. Under this circumstance,  $\Gamma$  versus intensity follows an inverse power law [ $\Gamma \propto I^{-\kappa}$ ]. As shown in Fig. 3-3(a), the value of  $\kappa$  is about 0.81 for the intensity beyond  $2 \text{ W/m}^2$ , which is much larger than the exponent of  $\kappa=0.5$  dominated by the trap mechanism. Thus, this result suggests a non-trap mechanism in  $\text{SnO}_2$  NWs. The mechanism responsible for the PC observed here may be attributed to the modulation of surface space charge region according to the

simulation of Muñoz et al and Garrido et al.<sup>15,17</sup> It predicts a power law dependence for the relationship between gain and excitation intensity with the value of  $\kappa$  in the range 0.5-0.9.

It is well-known for SnO<sub>2</sub> NWs with surface defects, usually oxygen defects, resulting in an n-type semiconductor.<sup>18</sup> Owing to the defects at the surface, the upward band-bending exists and forms a low-conductivity depletion layer at the surface referred to space charge region. Because NWs have much higher surface-to-volume ratio, the surface of NWs influences the conductivity more drastically. Once electron-hole pairs are photogenerated, holes drift to the surface readily surface electric field, leaving unpaired electrons inside, thus being spatially separated.<sup>18</sup> Thereupon, the recombination probability of electrons and holes reduces, and consequently the lifetime of conducting electrons increases. At the intensity of 100 W/m<sup>2</sup> as shown in Fig. 3-3(b), the PC contributed from surface band-bending is 81% and only 19% is from hole-trap effect.

However, the  $\kappa$  of “short rise time” PC is 0.5 as shown in Fig.3-4, which is believed that the PC is induced by the intrinsic recombination mechanism from bulk, and is not the focus here.

Let us now examine the PC response in vacuum condition. As shown in Fig. 3-5, when the SnO<sub>2</sub> NW is placed in a vacuum of 10<sup>-6</sup> torr for 30 min, the dark current is a little higher than that in air which can be explained by the existence of the oxygen adsorption. However, under the illumination with an intensity of 100 W/m<sup>2</sup>, the PC is greatly enhanced by up to one order of magnitude compared with that measured in air. Besides, both of the PC rise and decay times exhibit a much slower process. Quite remarkably, the gain now reaches an extremely high value of one hundred thousand. This behavior can be easily understood based on the reduction of adsorbed oxygen molecules on the NW surface. With the reduction of adsorbed oxygen molecules, the photoexcited electrons can now enjoy a longer lifetime, therefore all the rise and decay times are enhanced. As shown in Fig. 3-6(a), the high gains can be also obtained under different intensity, and in Fig. 3-6(b), the exponent  $\kappa$  is changed to 0.7, which implies the difference of surface band-bending in different ambient surrounding.

The SnO<sub>2</sub> NW device is also studied under green laser illumination (532nm) with light intensity 40000 W/m<sup>2</sup>, and the photoresponse in air was given in Fig. 3-7. As for the SnO<sub>2</sub> NW device, the current increases from 12.5 nA to 15nA on green light

illumination. As oxygen molecules are adsorbed on the surface of the SnO<sub>2</sub> NW, they capture electrons from the NW and form negatively charged ions. When light with energy below the band gap is introduced, the electrons captured at the oxygen molecules are photoexcited to the conduction band, which enhances the electron density and lowers the band-bending. Both of them give rise to the increase of conductance.





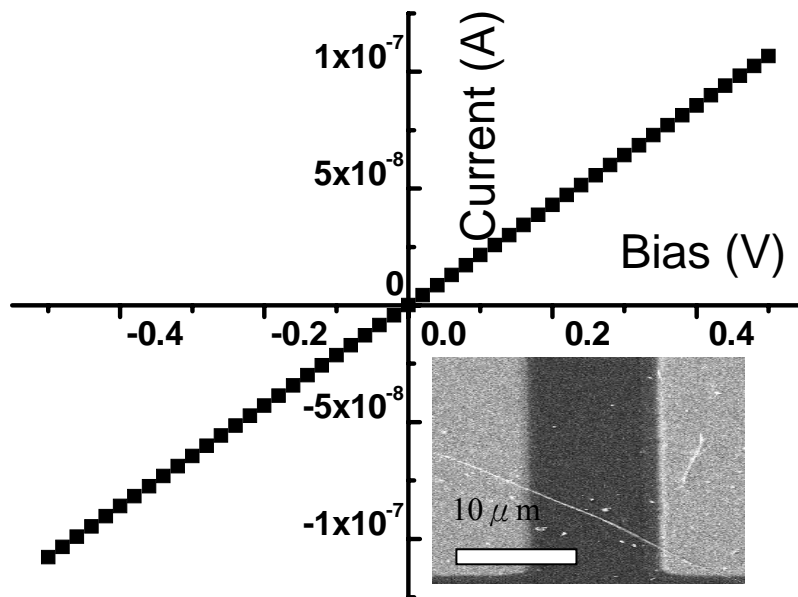


Fig. 3-1: *I-V* characteristics of SnO<sub>2</sub> nanowire in ambient air.

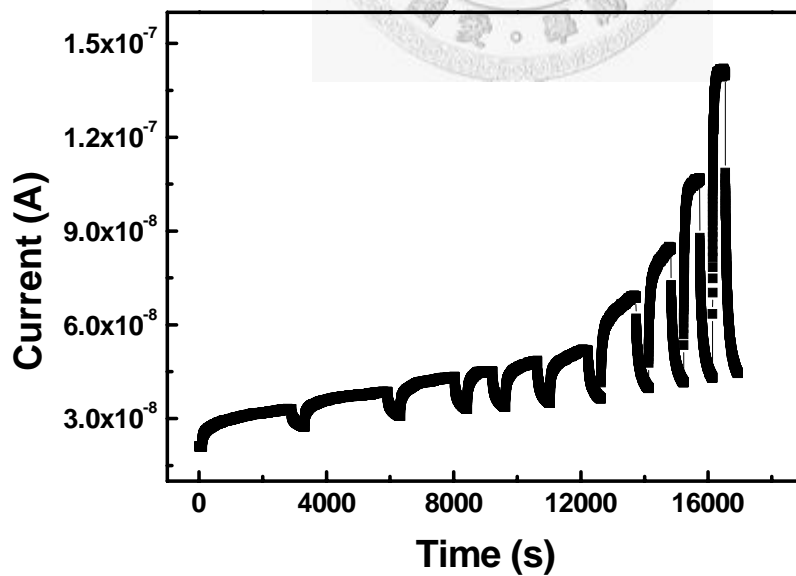


Fig. 3-2: Photocurrent of SnO<sub>2</sub> nanowire with a bias 0.1V under different excitation intensity.

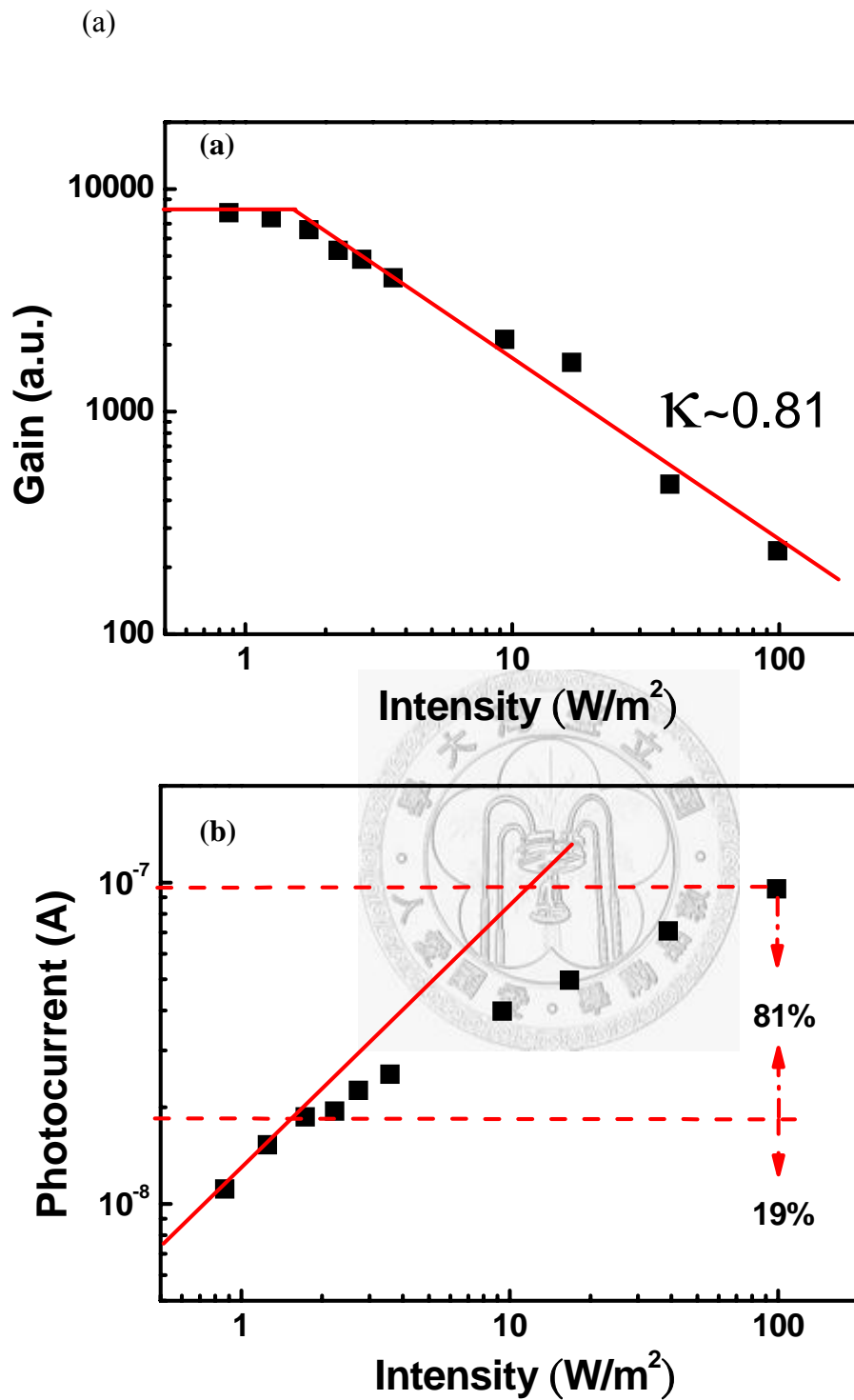


Fig. 3-3: (a) Photoconduction gain of  $\text{SnO}_2$  nanowire as a function of illumination intensity. (b) Photocurrent of a  $\text{SnO}_2$  nanowire as a function of excitation intensity.

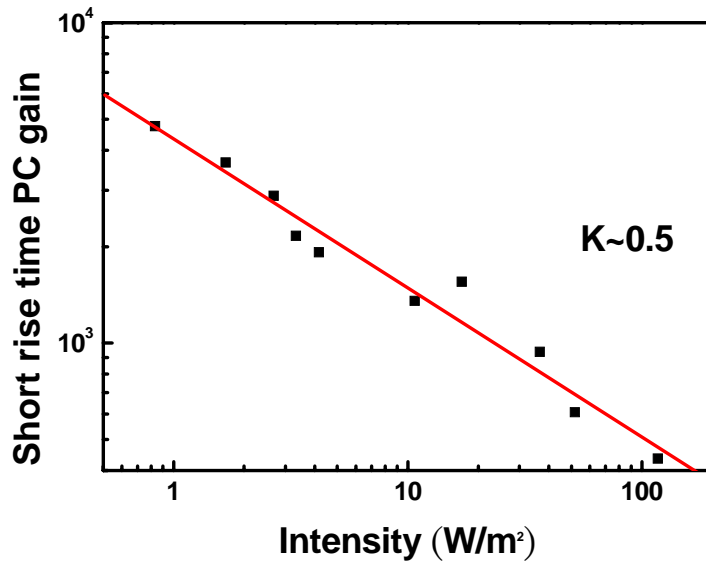


Fig. 3-4: Photoconduction gain of “short rise time” photocurrent versus different excitation intensity.

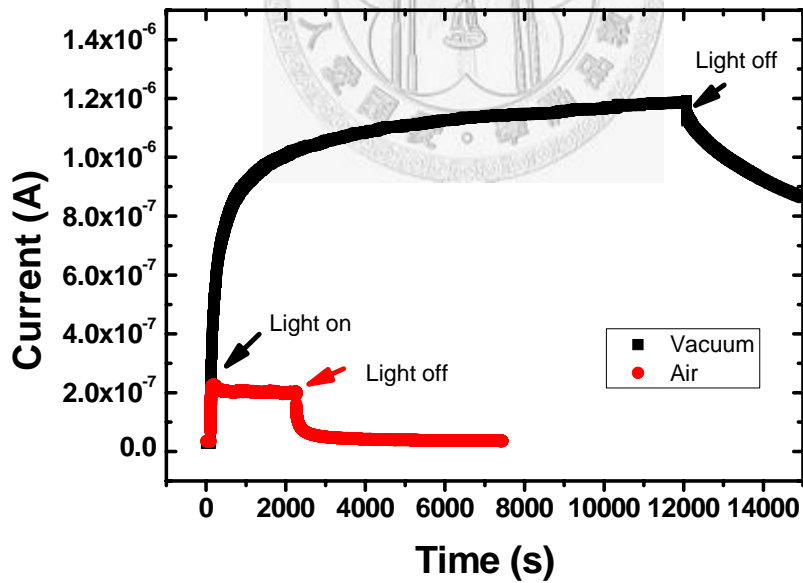
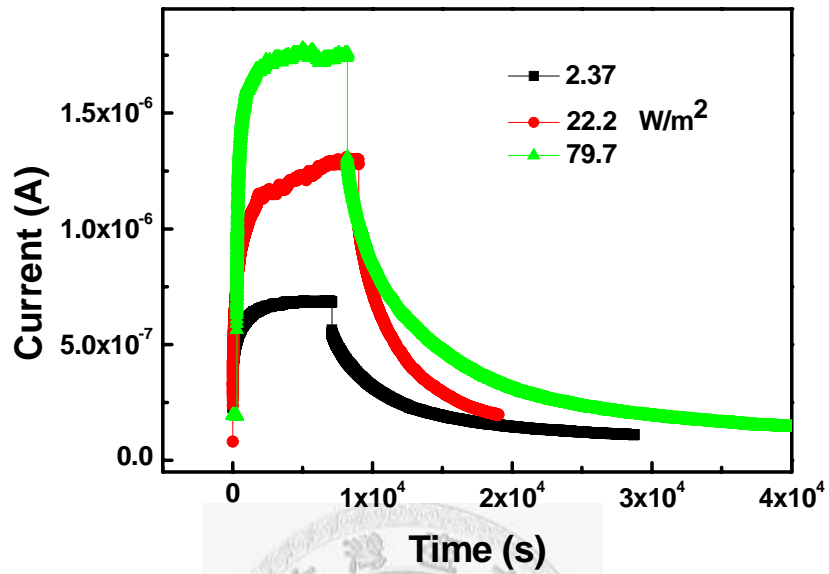


Fig. 3-5: Photocurrent of a  $\text{SnO}_2$  nanowire in air and in vacuum under the illumination of He-Cd laser with wavelength 325nm and excitation intensity of  $100 \text{ W/m}^2$  in vacuum.

(a)



(b)

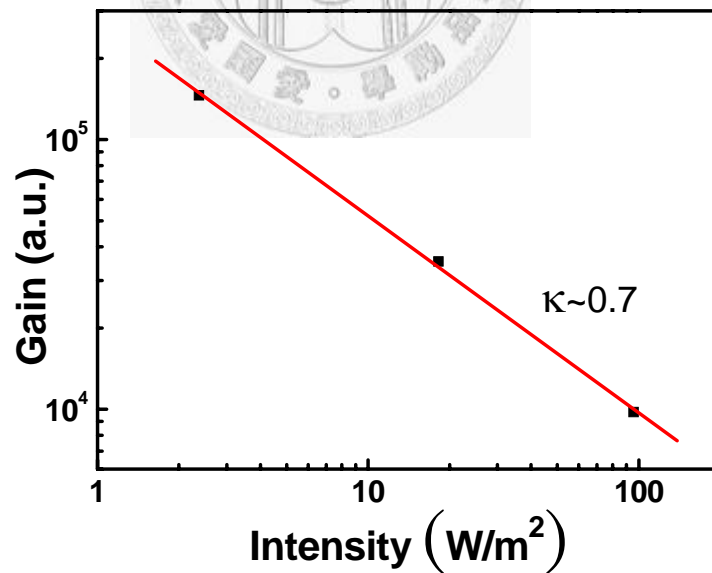


Fig. 3-6 (a) Photocurrent of a SnO<sub>2</sub> nanowire under the illumination of He-Cd laser with wavelength 325nm in vacuum. (b) Photoconduction gain relative to excitation intensity in vacuum.

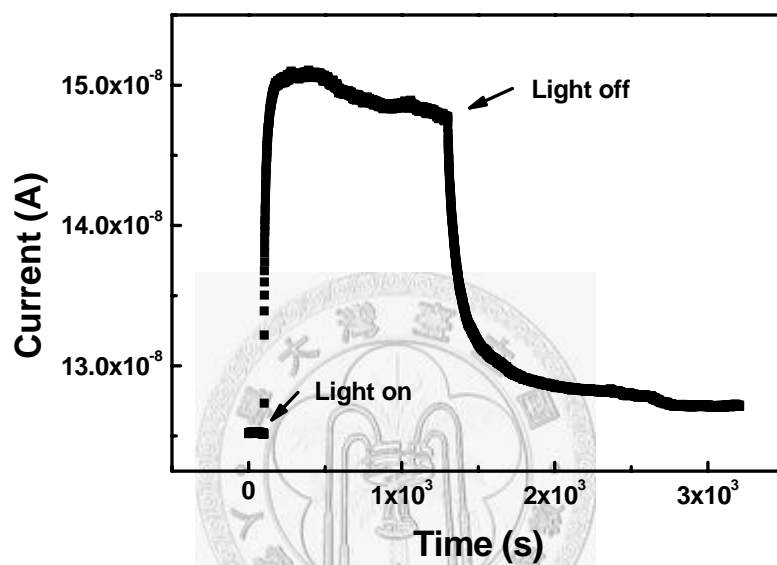
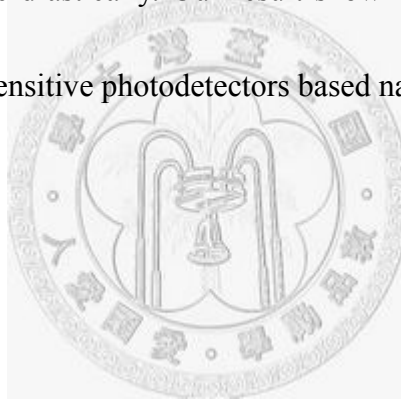


Fig 3-7: Photoresponse of the SnO<sub>2</sub> nanowire device under green laser illumination (532nm) with light intensity 40000 W/m<sup>2</sup>.

### 3-3 Summary

In summary, we have investigated the photoconductive properties in a SnO<sub>2</sub> NW, and quantified the gain of 10<sup>4</sup> in air and 10<sup>5</sup> in vacuum. Even the photocurrent in metal-oxide based 1D nanostructures has been studied for a long period, the responsible mechanism in previous reports always put emphasis on the neutralization of ionized oxygen molecules by trapping holes [ $h^+ + O_2^- \rightarrow O_2$ ]. Here we point out that the space charges induced by defects can also play a significant role, which can prolong the carrier lifetime drastically. Our result shown here should be very useful for the creation of highly sensitive photodetectors based nanostructured materials.



## References:

1. A. Andersson, N. Johansson, P. Broms, N. Yu, D. Lupo, and W. R. Salaneck, *Adv. Mater. (Weinheim, Ger.)* **10**, 859 (1998).
2. Y. Liu, C. Zheng, W. Wang, C. Yin, and G. Wang, *Adv. Mater. (Weinheim, Ger.)* **13**, 1883 (2001).
3. S. Luo, P. K. Chu, W. Liu, M. Zhang, and C. Lin, *Appl. Phys. Lett.* **88**, 183112 (2006).
4. B. Wang, Y. H. Yang, C. X. Wang, N. S. Xu, and G. W. Yang, *J. Appl. Phys.* **98**, 124303 (2005).
5. B. Wang, Y. H. Yang, C. X. Wang, and G. W. Yang, *J. Appl. Phys.* **98**, 073520 (2005).
6. S. Das, S. Kar, and S. Chaudhuri, *J. Appl. Phys.* **99**, 114303 (2006).
7. L. L. Fields, J. P. Zheng, Y. Cheng, and P. Xiong, *Appl. Phys. Lett.* **88**, 263102 (2006).
8. A. Yang, X. Tao, R. Wang, S. Lee, and C. Surya, *Appl. Phys. Lett.* **91**, 133110 (2007).
9. S. Choudhury, C. A. Betty, K. G. Girjia, and S. K. Kulshreshtha, *Appl. Phys. Lett.* **89**, 071914 (2006).
10. Q. H. Li, T. Gao, Y. G. Wang, and T. H. Wang, *Appl. Phys. Lett.* **86**, 123117

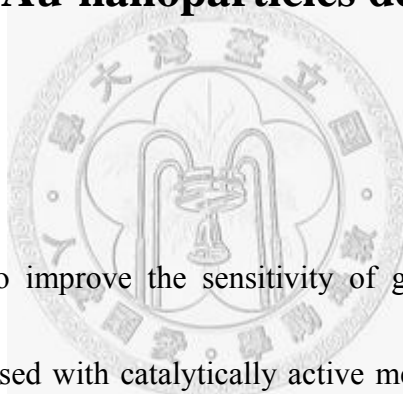
(2005).

11. Z. Liu, D. Zhang, S. Han, C. Li, T. Tang, W. Jin, X. Liu, B. Lei, and C. Zhou, *Adv. Mater. (Weinheim, Ger.)* **15**, 1754 (2003).
12. F. Hernandez-Ramirez, A. Tarancon, O. Casals, E. Pellicer, J. Rodriguez, J. R. Morante, S. Barth, and S. Mathur, *Phys. Rev. B* **76**, 085429 (2007).
13. R. S. Chen, H. Y. Chen, C. Y. Lu, K. H. Chen, C. P. Chen, L. C. Chen, and Y. J. Yang, *Appl. Phys. Lett.* **91**, 223106 (2007).
14. F. Binet, J. Y. Duboz, E. Rosencher, F. Scholz, and V. Härle, *Appl. Phys. Lett.* **69**, 26 (1996).
15. E. Muñoz, E. Monroy, J. A. Garrido, I. Izpura, F. J. Sánchez, M. A. Sánchez-García, E. Calleja, B. Beaumont, and P. Gibart, *Appl. Phys. Lett.* **71**, 870 (1997).
16. Y. Wang, I. Ramos, and J. J. Santiago-Aviles, *J. Appl. Phys.* **102**, 093517 (2007)
17. J. A. Garrido, E. Monroy, I. Izpura, and E. Muñoz, *Semicond. Sci. Technol.* **13**, 563 (1998).
18. X. T. Zhou, F. Heigl, M. W. Murphy, T. K. Sham, T. Regier, I. Coulthard, and R. I. R. Blyth, *Appl. Phys. Lett.* **89**, 213109 (2006).
- 19 R. H. Bube, *Photoelectronics Properties of Semiconductors*, (Cambridge, “New York, 1992), Chap. 2, pp. 21-30.



## Chapter 4

### Photocurrent enhancement of SnO<sub>2</sub> nanowires through Au-nanoparticles decoration

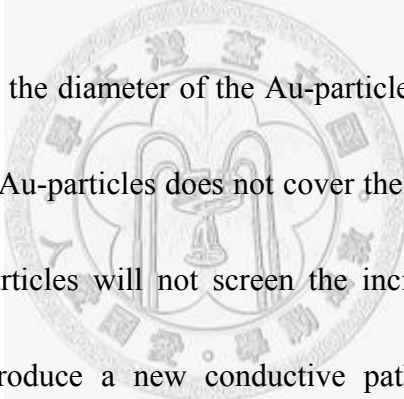


#### 4-1 Introduction

Currently, in order to improve the sensitivity of gas sensors, functionalizing materials have been proposed with catalytically active metals such as Pd and Ag on semiconductor NWs.<sup>10,11</sup> The metal particles on the surface will result in the formation of a localized Schottky junction, which creates a charge depletion region in the NWs in the vicinity of the metal particle. The metal-particles could become an intermediate in chemical combustion reactions which reduce the current through the NWs and then enhance the sensitivity. In this letter, we report that the photoresponse of SnO<sub>2</sub> NWs with Au-particles decorated can be enhanced. All our results can be interpreted based on the formation of the Schottky junction on the decorated surface.

## 4-2 Results and Discussion

A scanning electron microscopy (SEM) image of the sample is shown in the inset of Fig. 4-1. The distance of the channel between two terminals is  $10\ \mu\text{m}$ , and the diameters of the three NWs are respectively 137, 295, and 479 nm. The dark current versus bias ( $I$ - $V$ ) measurement is routinely checked to ensure Ohmic contact between nanowires and metal electrodes as shown in Fig. 4-1.



As shown in Fig. 4-2, the diameter of the Au-particles are about 10 nm, and the random distribution of the Au-particles does not cover the whole surface of the NWs. Thus the decorated Au-particles will not screen the incident light, and the excess Au-decoration will not produce a new conductive path on the surface and the substrate. As shown in Fig. 1, the  $I$ - $V$  curve of the NWs with the Au-particles is a little higher than that of the NWs with Au-particle. The dark current doesn't decrease by the expansion of SCRs after the Au-decoration because of the large density of conduction electrons in Au-nanoparticles. Figure 4-3 shows the results of photoresponse under different excitation intensity performed on SnO<sub>2</sub> nanowires in ambient air. It is obviously that the PC increases with increasing the light intensity from  $2.5\ \text{W/m}^2$  to  $1410\ \text{W/m}^2$ . Quite interestingly, when the nanowires are decorated

with Au-particles, the measured PC can be enhanced by up to about 110%. It will be intriguing to know the exact mechanism that causes the PC enhancement after Au-particles decoration. For the pristine SnO<sub>2</sub> nanowires studied here, the measured PC has an extremely high PC gain. Its value can reach up to about 900.

The high gain of SnO<sub>2</sub> is attributed to the presence of oxygen vacancies. Due to the existence of oxygen vacancies on the surface of the SnO<sub>2</sub> nanowires, the free electrons are accumulated on the surface.<sup>14</sup> Consequently, the existence of upward band-bending forms a low-conductivity depletion region at the surface referred to space charge regions (SCRs). After the electron-hole pairs are photogenerated, the photoinduced holes can migrate to the surface by the strong electric field. As a result, a conductive volume increment is produced. And the spatial separation of electrons and holes also reduce the electron-hole recombination rate, and therefore, the electron lifetime increases and the photoresponse is enhanced. According to the simulation of Garrido et al,<sup>14</sup> the PC induced by the modulation of surface SCRs causes  $\Gamma$  following the inverse law with excitation intensity, i.e.,  $\Gamma \propto I^{-\kappa}$ , and the exponent  $\kappa$  is between 0.5 and 0.9. As shown in Fig. 4-4, the gain logarithmic plot in the intensity ranging from 2.5 W/m<sup>2</sup> to 1410 W/m<sup>2</sup> shows a clear power law  $\kappa \sim 0.6$ , which is in good agreement with the decoration prediction.

Let us now try to understand the origin of the PC enhancement after the Au decoration. It is known that depositing the metallic particles on the surface of a semiconductor, such as SnO<sub>2</sub>,<sup>10,11</sup> results in a localized Schottky barrier in the vicinity of the metallic particles. The formation of the Schottky barrier on the surface will enhance the surface electric field and increase the width and height of space charge region as shown in Fig. 4-5. This is due to the fact that the work function of SnO<sub>2</sub> nanowires 4.7 eV, is smaller than that of Au cluster, 5.1 eV. The increase of the barrier height of the SCRs on the surface will enhance the spatial separation effect in illuminating process, and the electron lifetime is increased. In turn, the measured PC is enhanced. The exponent  $\kappa$  of inverse power law now changes from 0.6 to 0.65 as shown in Fig. 4-5 due to the enhancement of the SCRs on the surface of SnO<sub>2</sub> nanowires. This behavior can be simulated according to the following equations. SCRs inside a semiconductor produce a variation of the conductive volume when carriers are photogenerated, and the  $\Delta i$  can be expressed as

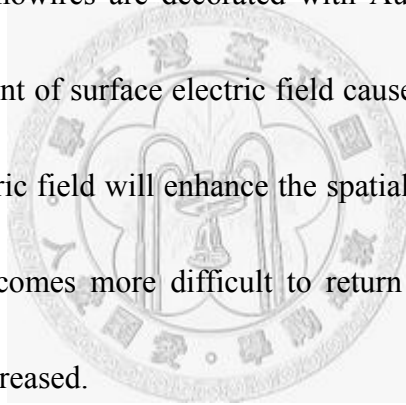
$$\frac{i_{dark}}{d - w_{dark}} \times \left\{ \left[ \frac{2\varepsilon\Delta\Psi_o}{qN_d} \right]^{1/2} - \left[ \frac{2\varepsilon(\Delta\Psi_o - \Psi_{ph})}{qN_d} \right]^{1/2} \right\}, \quad (4.1)$$

$$\text{where } V_{ph} = V_T \ln \left[ 1 + e^{\Delta\Psi_o/V_T} \left( q\eta \frac{P}{h\nu A^* T^2} \right) \right], \quad w_{dark} \approx \left( \frac{2\varepsilon\Delta\Psi_o}{qN_d} \right)^{1/2}. \quad (4.2)$$

$\varepsilon$  is the permittivity, and  $\Delta\Psi_o$  is the barrier height.  $N_d$  is the doping level,

$V_T = kT/q$ , and  $A^*$  is Richardson constant  $=1.2 \times 10^6 \text{ A/m}^2\text{K}^2$ .<sup>15</sup> Figure 4-6 shows the simulation results, which indicate the gain and the slope  $\kappa$  become larger with the increasing barrier height. This result is consistent with the Schottky junction model proposed as described above.<sup>11</sup>

Finally, as shown in Fig. 4-7, the decay time, that describes the photocurrent recovers to the dark current after turning off the incident light, increases from 112 s to 207 s, when the SnO<sub>2</sub> nanowires are decorated with Au particles. The behavior is consistent with enhancement of surface electric field caused by Au particles. Because the increased surface electric field will enhance the spatial separation of photoexcited electrons and holes, it becomes more difficult to return to the original states, and hence the decay time is increased.



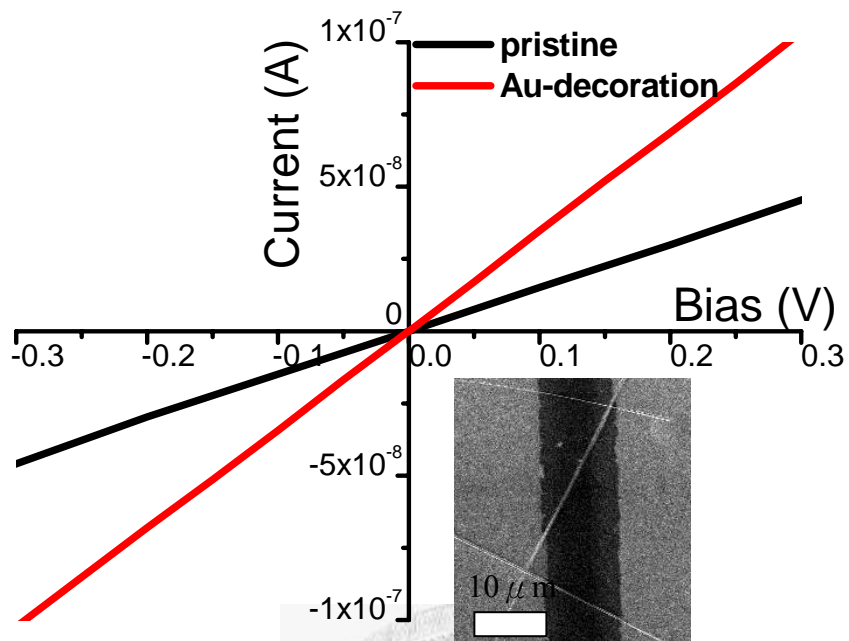


Fig. 4-1:  $I$ - $V$  characteristics of SnO<sub>2</sub> nanowires with and without Au-nanoparticles in ambient air.

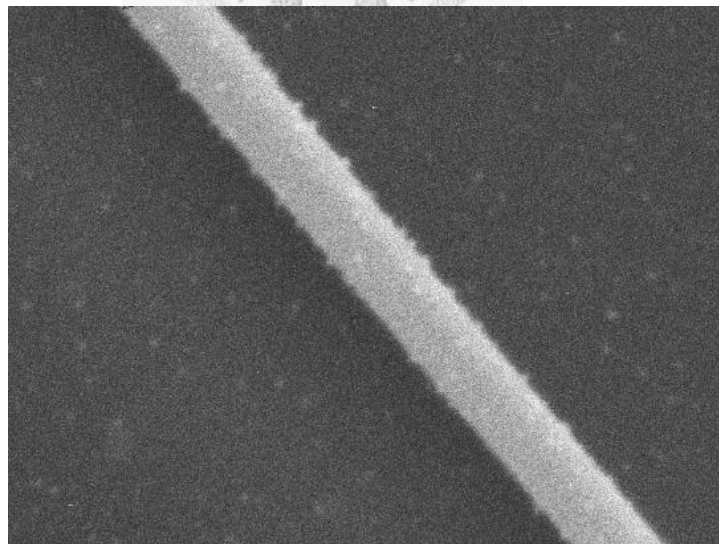


Fig. 4-2: Scanning electron microscope (SEM) image of the Au-decorated SnO<sub>2</sub> nanowires.

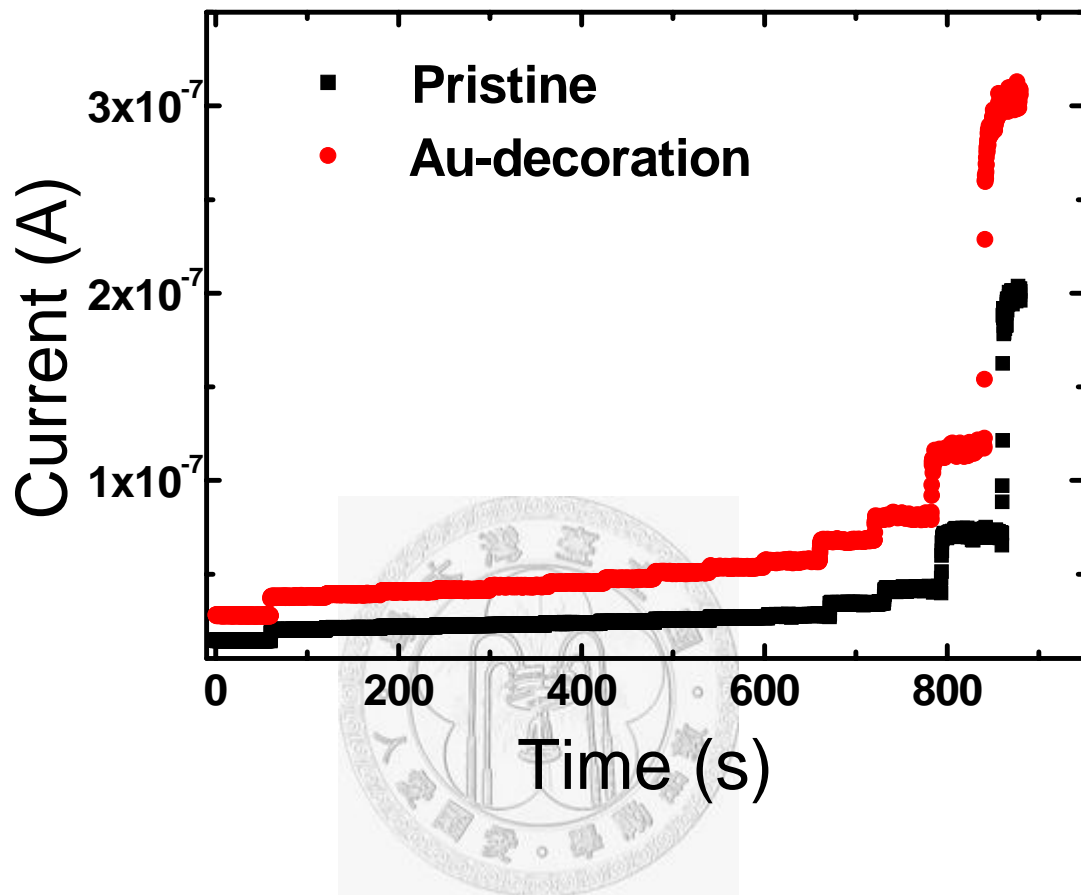


Fig. 4-3: Photoresponse of SnO<sub>2</sub> nanowires by UV illumination under different excitation intensity.

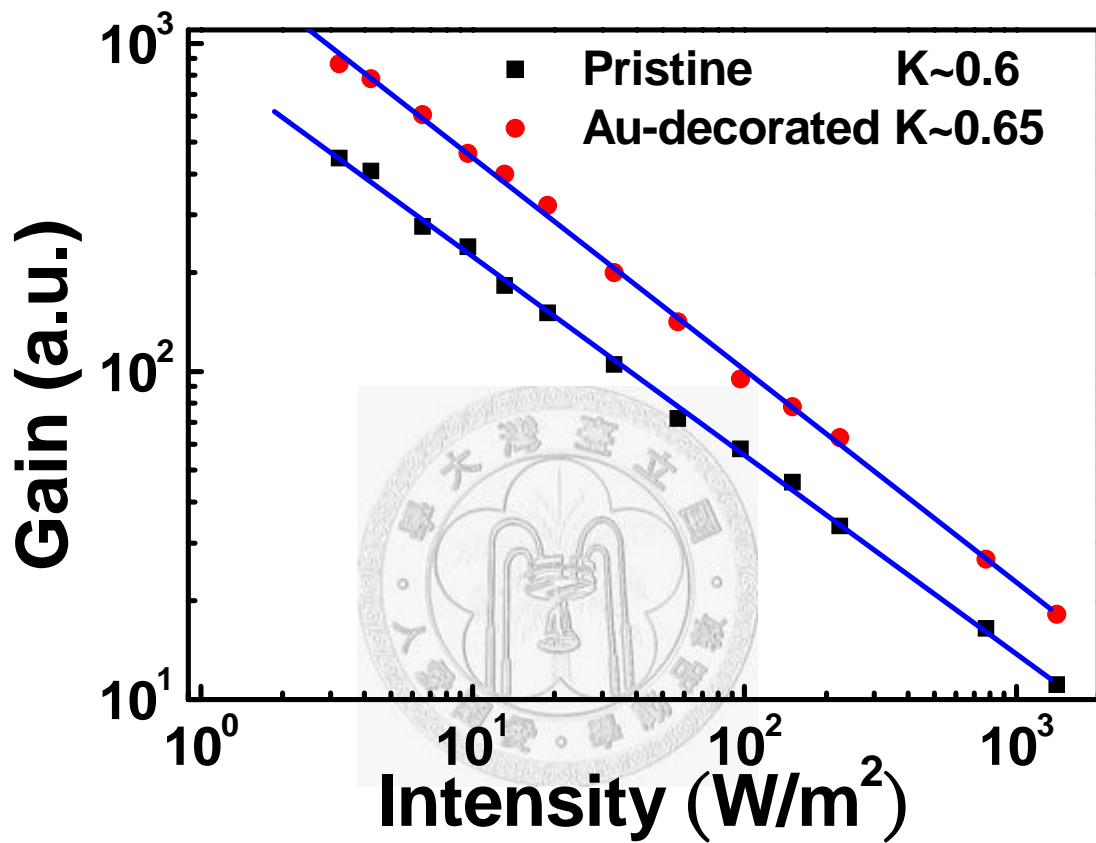


Fig. 4-4: Power dependence of pristine and Au-decorated SnO<sub>2</sub> nanowires.



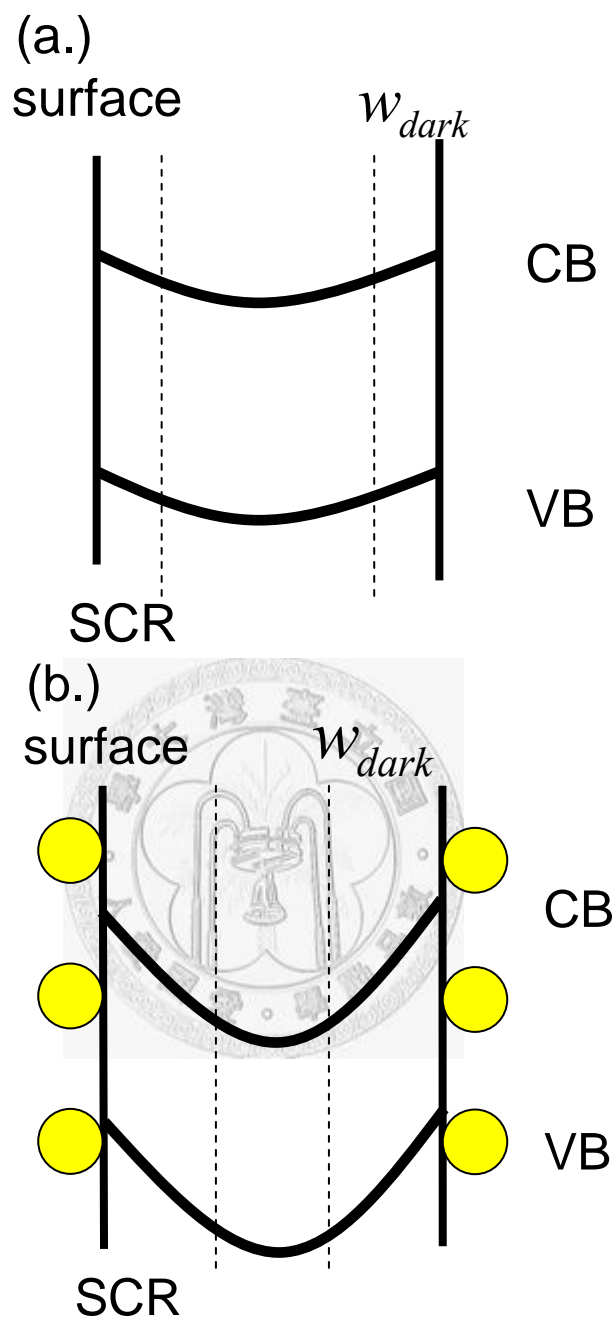


Fig. 4-5: (a.) Accumulation of free electrons and upward band-bending on the surface.

(b.) Au-nanoparticles result in a localized Schottky barrier in the vicinity of Au-nanoparticles, which will increase the height and the width of space charge region.

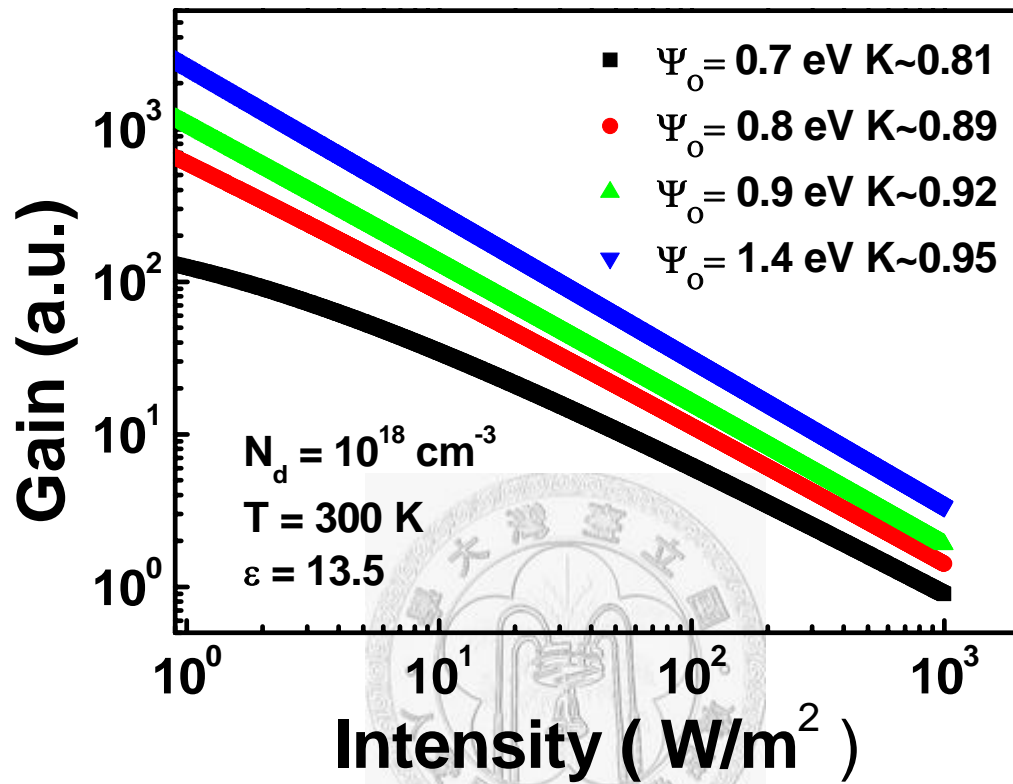


Fig. 4-6: Computer simulation of gain versus intensity and barrier height. An increase of the exponent  $\kappa$  and gain with increasing barrier height are obtained by this model.

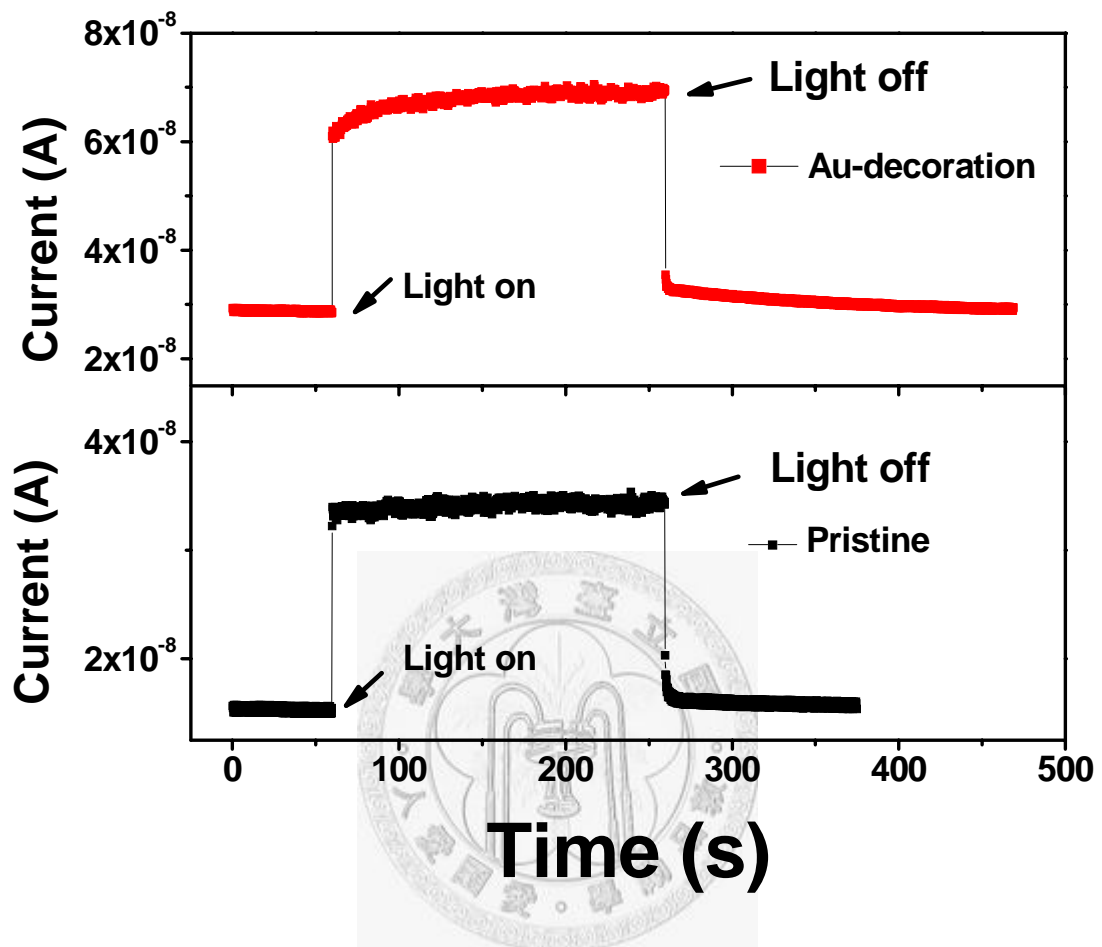
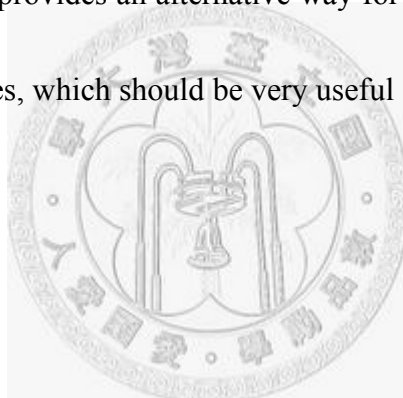


Fig. 4-7: Photocurrent measurement in (a) pristine and (b) Au-decorated  $\text{SnO}_2$  nanowires with an intensity of  $53 \text{ W/m}^2$ .

### 4-3 Summary

In summary, the metallic decoration has been utilized to improve the sensitivity of photoresponse in SnO<sub>2</sub> nanowires. The underlying mechanism is attributed to the formation of the localized Schottky barrier in the vicinity of metallic nanoparticles, which will enhance the surface electric field and increase the spatial separation of photoexcited electrons and holes. It thus prolongs the photoinduced electron lifetime, and increases the photocurrent gain. Our result therefore demonstrates that metal-particles decoration provides an alternative way for enhancing the photocurrent of semiconductor nanowires, which should be very useful for creating highly sensitive photodetectors.



## References

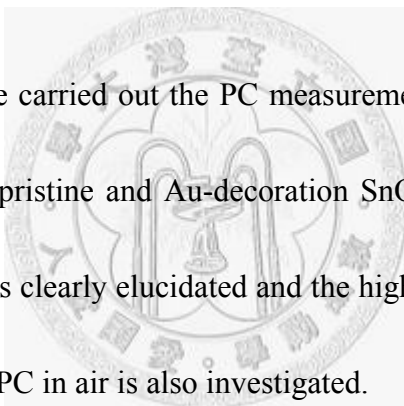
1. S. Dmitriev, Y. Lilach, Bradly. Button, M. Moskovits, and A. Kolmakov, *Nanotechnology*, **18**, 055707 (2007).
2. Z. Liu, D. Zhang, S. Han, C. Li, T. Tang, W. Jin, X. Liu, B. Lei, and C. Zhou, *Adv. Mater. (Weinheim, Ger.)* **15**, 1754 (2003).
3. Y. Liu, C. Zheng, W. Wang, C. Yin, and G. Wang, *Adv. Mater. (Weinheim, Ger.)* **13**, 1883 (2001).
4. B. Wang, Y. H. Yang, C. X. Wang, N. S. Xu, and G. W. Yang, *J. Appl. Phys.* **98**, 124303 (2005).
5. B. Wang, Y. H. Yang, C. X. Wang, and G. W. Yang, *J. Appl. Phys.* **98**, 073520 (2005).
6. S. Luo, P. K. Chu, W. Liu, M. Zhang, and C. Lin, *Appl. Phys. Lett.* **88**, 183112 (2006).
7. L. L. Fields, J. P. Zheng, Y. Cheng, and P. Xiong, *Appl. Phys. Lett.* **88**, 263102 (2006).
8. A. Yang, X. Tao, R. Wang, S. Lee, and C. Surya, *Appl. Phys. Lett.* **91**, 133110 (2007).
9. S. Choudhury, C. A. Betty, K. G. Girija, and S. K. Kulshreshtha, *Appl. Phys. Lett.* **89**, 071914 (2006).
10. A. Kolmakov, D. O. Klenov, Y. Lilach, S. Stemmer, and M. Moskovits, *Nano. Lett.* **5**, 667 (2005).
11. X. H. Chen, and M. Moskovits, *Nano. Lett.* **7**, 807 (2007).
12. F. Hernandez-Ramirez, A. Tarancon, O. Casals, E. Pellicer, J. Rodriguez, J. R. Morante, S. Barth, and S. Mathur, *Phys. Rev. B* **76**, 085429 (2007).
13. R. S. Chen, H. Y. Chen, C. Y. Lu, K. H. Chen, C. P. Chen, L. C. Chen, and Y. J. Yang, *Appl. Phys. Lett.* **91**, 223106 (2007).

14. X. T. Zhou, F. Heigl, M. W. Murphy, T. K. Sham, T. Regier, I. Coulthard, and R. I. R. Blyth, *Appl. Phys. Lett.* **89**, 213109 (2006).
15. J. A. Garrido, E. Monroy, I. Izpura, and E. Muñoz, *Semicond. Sci. Technol.* **13**, 563 (1998).



## Chapter 5

### Conclusion



In this thesis, we have carried out the PC measurements of SnO<sub>2</sub> NWs, and the difference of PC between pristine and Au-decoration SnO<sub>2</sub> NWs. The dominant PC mechanism of SnO<sub>2</sub> NWs is clearly elucidated and the high gain is peculiarly defined. A new way to enhance the PC in air is also investigated.

In chapter 3, PC of metal-oxide based one-dimensional nanostructures has been investigated for a long period, but the explication of PC mechanism always put emphasis on ionized oxygen molecules which can trap holes [ $h^+ + O_2^- \rightarrow O_2$ ] to increase the photoconductivity. Based on the power dependence in the thesis, we point out that band-bending effect also dominates the PC in air in SnO<sub>2</sub> NWs. Nevertheless, oxygen-deficient surrounding decreases the adsorption rate and prolongs the carrier

lifetime drastically, which increases the PC in one order of magnitude. The behavior of PC in air and in vacuum is consistent with previous references and all the metal-oxide semiconductors. This indicates the dominant mechanism of PC in metal-oxide semiconductors will change from hole-trap effect into surface band-bending when the environment is in oxygen deficiency.

In chapter 4, photoconductive measurements have been performed on SnO<sub>2</sub> nanowires with and without Au-nanoparticle surface decoration. The enhanced photosensitivity is attributed to the Schottky barrier effect. The increment in the barrier height of space charge region increases the spatial separation effect and prolongs the photoinduced electron lifetime. In turn, it increases the photocurrent gain. Our experimental results not only confirms the Schottky junction model used in improving gas sensing, but also provides a new way to enhance the photocurrent of semiconductor nanowires.

Finally, based on the investigation shown here, it is stressed that a precise picture photoresponse in metal-oxide based 1D nanostructured semiconductors has been established. Besides, a new route to increase the efficiency of photoresponse in 1D nanostructures based upon Au-nanoparticles decoration has been provided. These



results should be very useful for the future development of highly efficient optoelectronic devices.

